AD-A091 700 DIRECTORATE OF AEROSPACE STUDIES KIRTLAND AFB NM F/G 15/7
AIRBORNE PLATFORMS VERSUS AIRBREATHING STRATEGIC THREATS, A PER--ETC(U)
JUN 80 C L BOHN, A F COOPER, B J MANZ
UNCLASSIFIED DAS-TR-80-2 NL

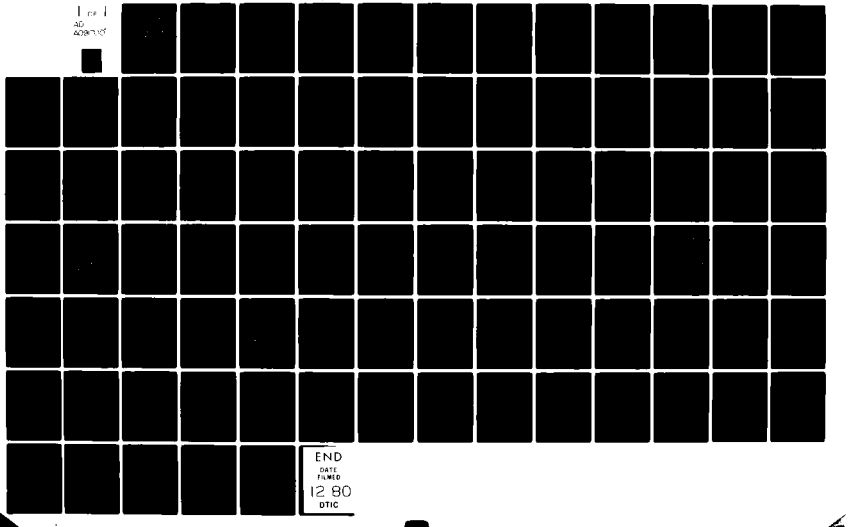

END
DATE FILMED
12 80
DTIC

DAS-TR-80-2 LEVEL II (12) B.S. DAS-TR-80-2

AIRBORNE PLATFORMS VERSUS AIRBREATHING STRATEGIC THREATS - A PERFORMANCE ASSESSMENT METHODOLOGY

JUNE 1980

1LT COURTLANDT L. BOHN, USAF
MR. A. FOSTER COOPER
DR. BRUNO J. MANZ

DIRECTORATE OF AEROSPACE STUDIES
DCS/PLANS AND PROGRAMS, HQ AFSC
KIRTLAND AFB, NEW MEXICO 87117

This paper presents a new methodology for assessing the performance of area defense weapon systems against airbreathing strategic threats. The methodology is probabilistic rather than simulative. It intertwines surveillance sensor, interceptor, and command, control and communications network. Furthermore, it allows for incorporating the propensity of the airbreathing threats to maneuver. The probabilistic approach provides the tools for direct sensitivity analyses against overall weapon system performance including tracking errors. The approach is amenable to direct interceptor scheduling and yields closed-form solutions, thus permitting relatively easy (and inexpensive!) programming.

The analytical presentation of the model is supplemented by a computerization and a numerical example.

The authors thank Ms Eileen Yankee and Ms Lois MacMenigall for preparing the manuscript, and Mr Jack Bennett for drawing the figures.

COURTLANDT L. BOHN, 1Lt, USAF
Staff Physicist
Directorate of Aerospace Studies

This report has been reviewed and is approved for publication.'

BRUNO J. MANZ, Assistant Chief
Studies & Evaluation Division
Directorate of Aerospace Studies

PAUL J. VALLERIE, Lt Col, USAF
Director of Aerospace Studies
DCS/Plans and Programs, HQ AFSC

This report has been reviewed by the Information Office (OI) and is releaseable to the National Technical Information Service (NTIS). At NTIS, it will be available to the general public, including foreign nations.

UNCLASSIFIED

SECURITY CLASSIFICATION OF THIS PAGE (When Data Entered)

REPORT DOCUMENTATION PAGE	READ INSTRUCTIONS BEFORE COMPLETING FORM
1. REPORT NUMBER: DAS-TR-80-2 / 2. GOVT ACCESSION NO.: AD-A092 700	3. RECIPIENT'S CATALOG NUMBER
4. TITLE (and Subtitle): AIRBORNE PLATFORMS VERSUS AIRBREATHING STRATEGIC THREATS, A PERFORMANCE ASSESSMENT METHODOLOGY	5. TYPE OF REPORT & PERIOD COVERED: Final Rept Jan - Jun 1980
	6. PERFORMING ORG. REPORT NUMBER
7. AUTHOR(s): Courtlandt L. Bohn, A. Foster Cooper, Bruno J. Manz	8. CONTRACT OR GRANT NUMBER(s)
9. PERFORMING ORGANIZATION NAME AND ADDRESS: Directorate of Aerospace Studies, Kirtland AFB, NM 87117	10. PROGRAM ELEMENT, PROJECT, TASK AREA & WORK UNIT NUMBERS
11. CONTROLLING OFFICE NAME AND ADDRESS	12. REPORT DATE: June 1980
	13. NUMBER OF PAGES: 115
14. MONITORING AGENCY NAME & ADDRESS (if different from Controlling Office)	15. SECURITY CLASS. (of this report): UNCLASSIFIED
	15a. DECLASSIFICATION/DOWNGRADING SCHEDULE

16. DISTRIBUTION STATEMENT (of this Report)

Approved for public release; distribution unlimited.

17. DISTRIBUTION STATEMENT (of the abstract entered in Block 20, if different from Report)

18. SUPPLEMENTARY NOTES

19. KEY WORDS (Continue on reverse side if necessary and identify by block number)

Strategic Defense
Airbreathing Threats
Airborne Platforms
Applied Probability Theory
Air-to-Air Engagement
Distribution Functions
Homing Simulation

20. ABSTRACT (Continue on reverse side if necessary and identify by block number)

This paper presents a new methodology for assessing the performance of area defense weapon systems against airbreathing strategic threats. The methodology is probabilistic rather than simulative. It intertwines surveillance sensor, interceptor, and command, control and communication network. Furthermore, it allows for incorporating the propensity of the airbreathing threats to maneuver. The probabilistic approach provides the tools for direct sensitivity analyses against overall weapon system performance including tracking errors. The approach is amenable to direct interceptor

DD FORM 1 JAN 73 1473 EDITION OF 1 NOV 65 IS OBSOLETE

UNCLASSIFIED

SECURITY CLASSIFICATION OF THIS PAGE (When Data Entered)

20 scheduling and yields closed-form solutions, thus permitting relatively easy (and inexpensive) programming.

The analytical presentation of the model is supplemented by a computerization and a numerical example.

MODEL OVERVIEW

This model is designed to support an analysis, the objective of which is to determine the potential of candidate air defense engagement systems to counter a Soviet airbreathing attack against the continental United States in the 1985-2010 time frame. One class of engagement systems centers on area defense with an air-based weapon platform. This is the class the Airborne Platforms Versus Airbreathing Strategic Threats (APVAST) model treats. A possible measure of merit centers on expected number of penetrators negated, $< N_K >$. By combining salient features of interceptor, sensor, penetrator, and command, control, and communications (C^3), the APVAST methodology leads to a calculation of expected kill probability, $<P_K>$, from the conventional kill probability, P_K, which in turn gives $< N_K >$. The methodology is probabilistic rather than simulative and is adaptable to either an abstract treatment of scenarios or to a full-blown, concrete campaign model.

A standard approach to modelling air defense problems involves Monte Carlo techniques. It requires as the initial input a concrete campaign laydown, wherein individual penetrators are explicitly assigned to individual targets. By exercising the model many times, the user can calculate expected values and corresponding distribution functions directly. While the Monte Carlo techniques are straightforward and easy to understand, they invariably lead to inefficient, i.e., time-consuming, software. In turn, sensitivity analyses become expensive.

These drawbacks are altogether avoided using probabilistic techniques. These techniques are analytically demanding and less intuitive, but they lead to a model which, when exercised only once, is equivalent to an infinite number of Monte Carlo runs. The model can accept abstract weapons laydown as an input, and it also can accept a concrete laydown. It is a tool for doing immediate sensitivity analyses.

The basic APVAST goal is to convert conventional kill probability into expected kill probability. The principle for doing so is elementary. Every sensor reading is subject to uncertainties. Since a sensor measures both

penetrator position and velocity, there are six uncertainties, one for each of the three position degrees-of-freedom and one for each of the three velocity degrees-of-freedom. With each of the six uncertainties is associated a corresponding distribution function. For example, if the uncertainties are all Gaussian, then each of the associated distributions is Gaussian, and the penetrator is "centered" within a six-dimensional Gaussian ellipsoid. (The ellipsoid set up by the three position uncertainties is called an "error basket.") As long as a penetrator remains within sensor coverage, the ellipsoidal axes are determined solely from sensor parameters depending on the penetrator spacing. However, once the penetrator leaves sensor purview, its position uncertainty grows with time and, consequently, the corresponding expected kill probability shrinks through the growing uncertainty inherent in the interceptor's vectoring information.

Two other factors affect the accuracy of the vectoring information. One is the C^3 network. For example, the C^3 network may allow for continuous update, periodic update, or no update of the interceptor's vectoring instructions, and the $< P_K >$ shrinks correspondingly. As a case in point, if the C^3 cannot allow for vectoring update, then intercept is driven solely by the last available sensor reading. The corresponding error basket will have grown from the time of the last sensor reading up to the attack time with the concomitant shrinking of $< P_K >$, just as it would when the penetrator leaves sensor coverage. Another important C^3 property is inherent dead time. For non-zero dead time, the vectoring instructions are based on "dated" sensor readings.

The other important factor affecting the error basket is penetrator maneuvers. Once sensor readings become unavailable and the error basket begins to grow, that growth is further exaggerated by penetrator maneuvers. The error basket becomes "warped", i.e., no longer Gaussian, and because it is larger, penetrator maneuvers serve to further degrade $< P_K >$. Though the calculation is difficult, the warped error basket can be analytically determined through a series of convolutions (integrations) over the sensor-induced and maneuver-induced distribution functions.

The $< P_K >$ calculation against a given penetrator also hinges on determining the expected attack time, $< t_A >$, and corresponding expected attack position, $< \vec{r}_A >$, to which the interceptor flies to attack the penetrator based on its vectoring instructions. This calculation impacts P_K which, in turn, impacts $< P_K >$. If the penetrator does not maneuver, then $< t_A >$, $< \vec{r}_A >$ arise through elementary vector analysis. If, on the other hand, the penetrator does maneuver, then (given vectoring information update) these maneuvers drive the interceptor to maneuver and home for kill. The probabilistic approach offers a natural framework within which to account for this homing.

In summary, an alternative to Monte Carlo techniques is now available for air defense modelling. The key is a probabilistic approach through which interceptor, sensor, C^3, and penetrator properties can be immediately tied together to provide a completely analytical solution for $< P_K >$. At user's discretion, the methodology can be applied either abstractly or in a concrete campaign model, and its flexibility allows for sensitivity analyses to both performance parameters and scenarios.

TABLE OF CONTENTS

LIST OF ILLUSTRATIONS

I. INTRODUCTION

The defense of our land-based strategic forces against the airbreathing leg of the Soviet triad is a major driver of current Air Force development planning activities. One manifestation is the November 1979 tasking of the Directorate of Aerospace Studies (office symbol AFCMD/SA) by Headquarters Air Force Systems Command (AFSC) to support an AFSC Air Defense Mission Analysis. The major analysis objective is to determine the potential of candidate surveillance and engagement systems to protect the continental United States from the 1985-2010 Soviet airbreathing threat. For the usual cost-effectiveness assessment, it is first necessary to quantify the effectiveness of a large number of systems and system combinations. For the initial screening, AFCMD/SA has chosen as measure of merit the number of penetrators killed, $< N_k >$. The objective is all-encompassing; sensors could be in any basing mode from ground-based through space-based and could rely on any one of several advanced technologies, while far-term interceptors could be designed for either area defense or terminal defense, or could have a layered defense profile, and could also be in any basing mode. This paper concentrates on area defense systems, one leg of which is constituted by mobile airborne weapon platforms. It presents a methodology for quantifying the performance of the entire defense system consisting of sensors, interceptors, and command, control, and communications (C^3) capabilities.

The generic scenario under study is represented in figure 1. A raid of strategic airbreathing penetrators originates from home bases, penetrates a tactical warning fence, proceeds to the targets, and then heads for recovery bases. Their goal is to attack all targets at the same time to avoid early tactical warning induced by early weapon detonation. Each raid member penetrates from a highly favored direction; for example, the most favored direction of a bomber raid penetrating the Distant Early Warning Line is obviously from north to south. The distance from the home base to the point of fence penetration is denoted R_{BF}; the distance from the point of fence

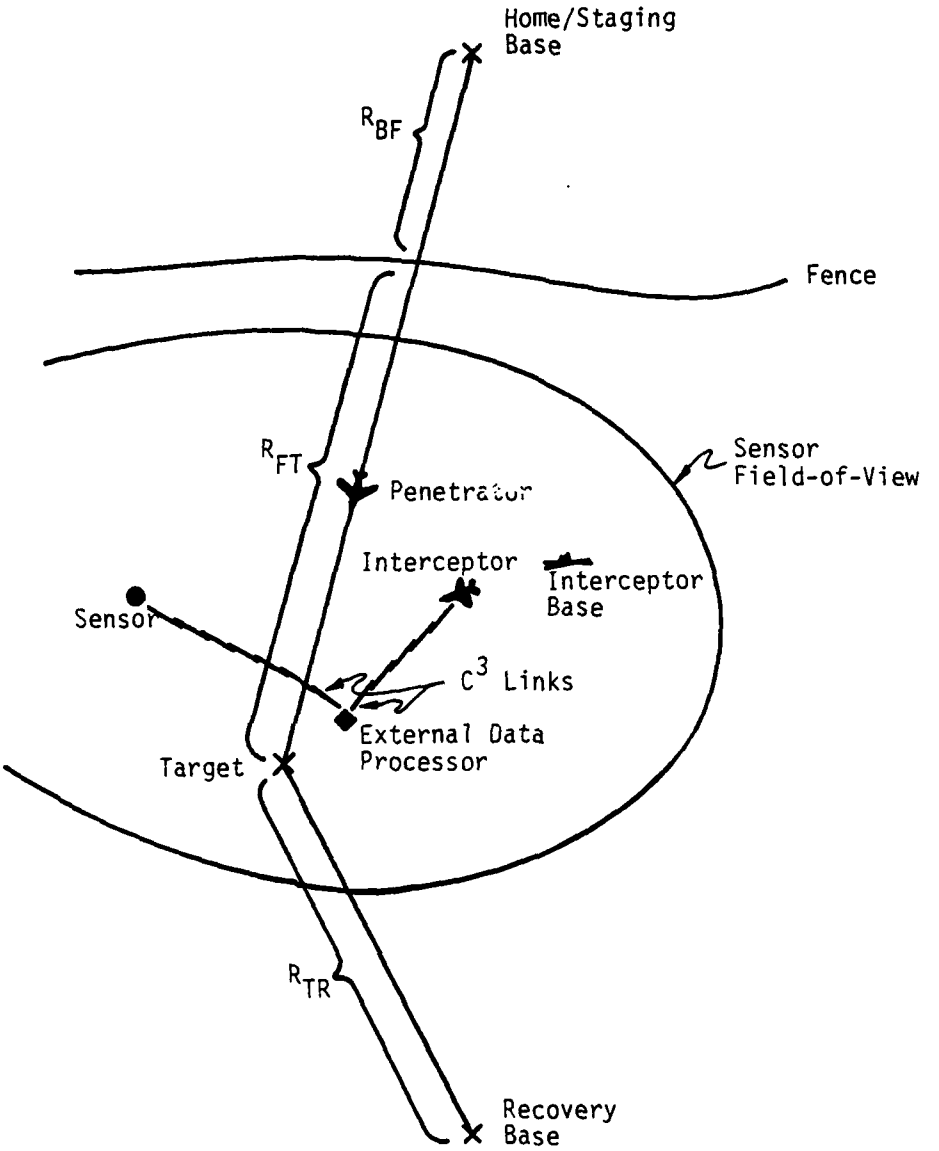

Figure 1. Schematic Outline of the Problem

penetration to the target is R_{FT}; and the distance from the target to the recovery base is R_{TR}. Clearly, if the individual penetrator is to recover safely, then the sum of R_{BF}, R_{FT}, and R_{TR} cannot exceed the total range capability R_P of the penetrator. Impeding the attack is an active defense system consisting of the tracking sensor, C^3 network, and interceptor. Generally these elements are separate; however, in certain revolutionary concepts they may be collocated, in which case the interceptor becomes autonomous. This "trio" of subsystems comprising the total defense system presents a rather difficult modelling problem which is further complicated by the fact that an airbreathing penetrator can maneuver by changing its heading, or its speed, or both.

A Monte Carlo approach would lead to an excessive number of cases, while the simple simulation of one "representative" case would be so strongly biased that the results would be worthless. Both pitfalls are avoided by the probabilistic approach which, however, is analytically demanding.

The essence of the probabilistic approach is brought out by the following considerations. A sensor reading indicating position, speed, and heading has associated errors, or standard deviations. As the penetrator proceeds to the target, these errors cause the position uncertainty to grow in a quantifiable way; maneuvers worsen the position uncertainty. The magnitude of the position error at the intended time of intercept also depends on C^3 capabilities, that is, on the dead time between sensor reading and relaying of vectoring information. Finally, the expected probability of kill, $\langle P_K \rangle$, depends on both the position uncertainty at the intended time of intercept and on the interceptor capabilities. Given fixed interceptor capabilities, a larger position uncertainty results in a smaller $\langle P_K \rangle$.

For optimal scheduling of the mobile intercept force, it is necessary to know the times at which and the positions from which the penetrators are attacked. Moreover, to insure that a penetrator is killed before it can attack its assigned target, one also needs to know the time and position of kill. These requirements are met by an approach which models interceptor homing. Of course, this approach has to account for penetrator maneuvers. All of these requirements are satisfied in the most natural way by the probabilistic approach.

The following sections develop the probabilistic methodology. Section II develops the necessary tools for quantifying the growth of both sensor-induced and maneuver-induced position uncertainties, and it discusses how to use these tools to calculate $<P_K>$. Section III lays out the basic equations which couple attack geometry and interceptor capabilities without allowing for maneuvers. The tools developed in section II and the basic equations of section III form the foundation for section IV which folds in penetrator maneuvers to describe interceptor homing, subject to C^3 capabilities. Section V provides an example to demonstrate the model's adaptability; it describes modelling of an air defense system which centers on standoff guided air-to-air missiles (AAMs) -- an at least conceptually possible alternative. The theory concludes with section VI which sketches the logical steps required to determine expected number of penetrators negated. Tedious calculations are relegated to the appendices. Appendix A discusses the transformation of standard deviations from one coordinate system to another. Appendix B presents an approximate solution of an integral surfacing in section II. Appendix C presents the APVAST program and serves as an abbreviated user's manual. The reader who needs only to know how to the use the program is referred directly to Appendix C.

The model has been computerized. Appendix C offers the listing of the computer program, a list of translation of the symbols of the theory into computer language, and a numerical example in input-output form.

II. PROPAGATION OF POSITION UNCERTAINTY

Measurements are always subject to uncertainty and are generally associated with distribution functions. In the present problem, penetrator position uncertainty arises initially due to sensor imperfections. As time passes on, and the penetrator proceeds to the target, the position uncertainty evolves due to three factors -- penetrator motion. sensor motion, and penetrator maneuvers. This section develops the tools needed to quantify this evolution. It begins with a discussion of the distribution functions pertaining to the initial measurements. It then calculates the evolution of the final position distribution functions. Thereafter, it turns to the use of the position distribution functions in calculating $\langle P_K \rangle$.

A. INHERENT DISTRIBUTION FUNCTIONS

1. Problem Schematics. The geometry of the air defense problem provides a natural framework for characterizing the inherent distribution functions. Figure 2 shows an overhead view of the problem geometry assuming a flat earth. The justification for neglecting the earth's curvature lies in the fact that the engagement of penetrators by sensors and interceptors, due to the limited range of the latter, always takes place within dimensions which are small compared to the earth's radius. In figure 2, an interceptor air base (AB) serves as the origin for the cartesian reference system (x,y,z). The y-axis is aligned toward the most favored direction from which the raid is coming. For concreteness, that direction is taken to be north. Centered on the sensor (S) is the sensor-based cartesian system (x_S,y_S,z_S).

Also shown in figure 2 is the tactical warning fence F. It separates the defended from the undefended airspace. The basic assumption is that the penetrator will not maneuver before it reaches the fence, but it generally will maneuver thereafter. The penetrator trajectory originates from the home base P_H, penetrates the fence at the point P_F, and proceeds to the target P_T. Whereas the trajectory section from P_H to P_F is straight by assumption, the section from P_F to P_T is generally curved due to maneuvers. In figure 2, the curved path from P_F to P_T is an example of an actual penetrator trajectory.

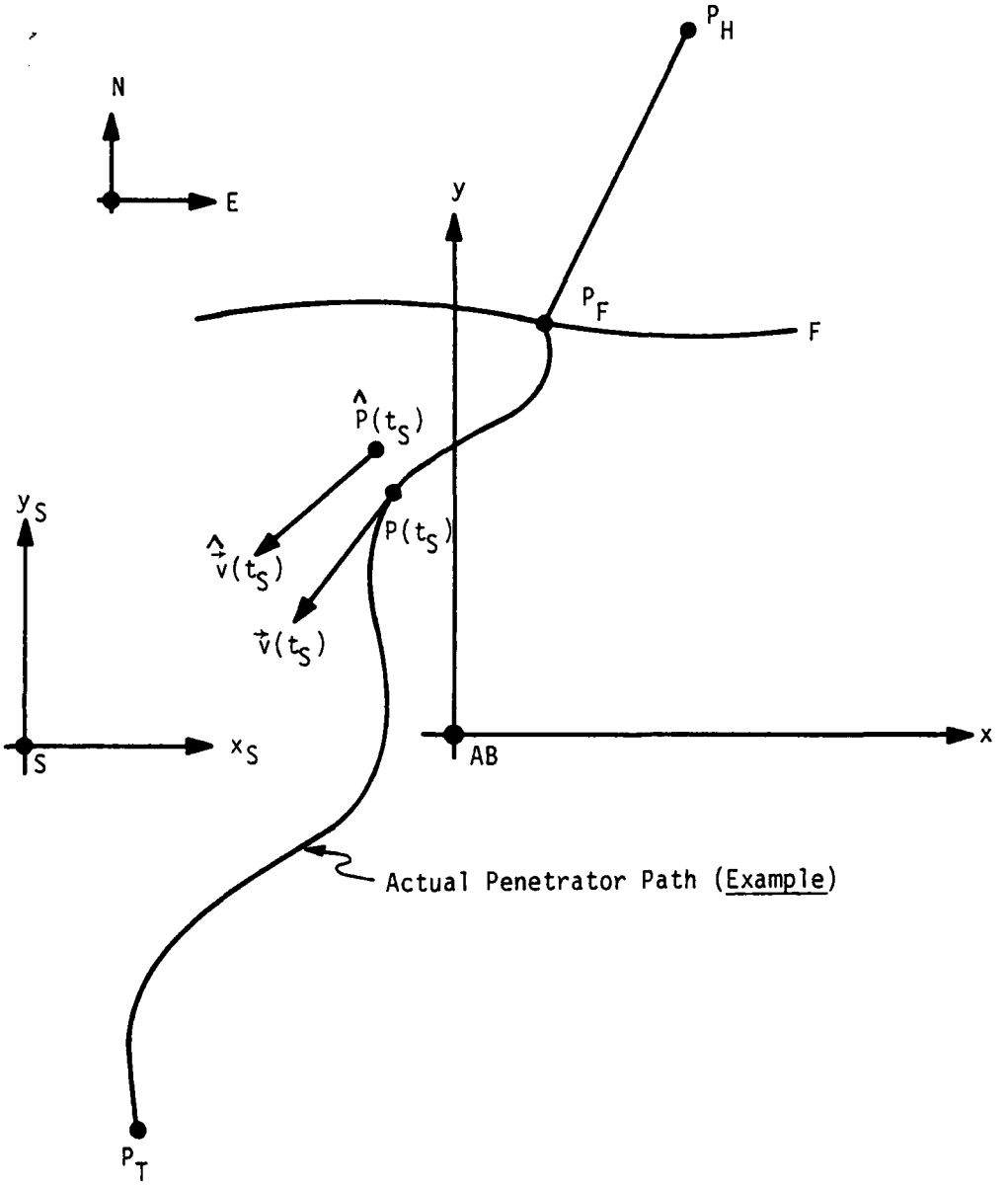

Figure 2. Problem Geometry, Overhead View

At some time t_S, the sensor peforms an observation, or measurement. At this time, the penetrator occupies some postion $P(t_S)$ on the curved path, and has some velocity $\vec{v}(t_S)$, as is shown in figure 2. The sensor-determined penetrator position and velocity are $\hat{P}(t_S)$ and $\hat{\vec{v}}(t_S)$, also shown in figure 2. Generally, due to sensor imperfections, $\hat{P}(t_S)$ and $\hat{\vec{v}}(t_S)$ will deviate from $P(t_S)$ and $\vec{v}(t_S)$.

It is now important to understand the following. If somebody measures an unknown quantity, say x, and quotes the result of his measurement, he always quotes that value of x which, in his mind and with regard to his information, is the "most probable" value of x. If we denote this value by <x|Inf>, then we may say that this is the result of the measurement which yielded the information listed in the condition compartment.

These conditions apply to the sensor-observed data $\hat{P}(t_S)$ and $\hat{\vec{v}}(t_S)$. They are, <u>from the point of view of the sensor</u>, the most probable penetrator position and velocity at the time t_S.

2. <u>Perturbation Approach</u>. On the trajectory section from P_F to P_T, the penetrator generally maneuvers. Therefore, the trajectory section is generally not straight. However, in the absence of any information about the actual maneuvering, the expected, or average, trajectory is a straight line. This expected trajectory is shown in figure 3, where it is labeled L. Clearly, L is the continuation of the straight line from P_H to P_F.

The gist of the perturbation approach is the following. The sensor-observed position $\hat{P}(t_S)$ is the most probable penetrator position from the point of view of the sensor, but not from the point of view of the analyst. In fact, from the analyst's point of view, $\hat{P}(t_S)$ is simply an unknown sample value. What, then, is the most probable sensor-determined penetrator position from the point of view of the analyst? Here the straight line L from figure 3 comes into play. This is the expected, or average, trajectory. From the analyst's point of view, it is the most probable trajectory. Therefore, from the analyst's point of view, the most probable sensor-determined penetrator position at some given time t_o lies on L.

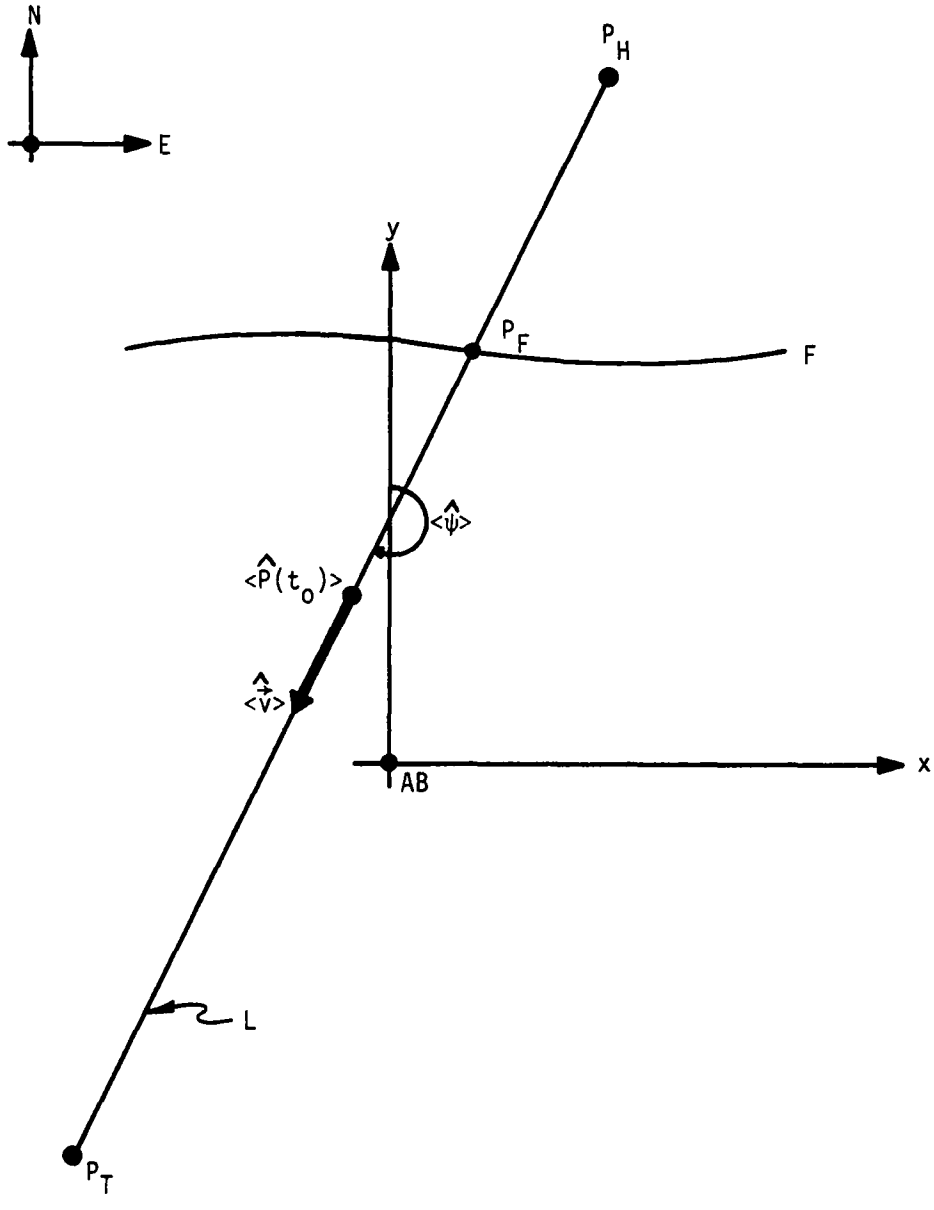

Figure 3. Expected Penetrator Path

It is for these reasons that the perturbation approach replaces the unknown sample value of the sensor-determined penetrator position, $\hat{P}(t_s)$, by a suitably selected point $\langle\hat{P}(t_0)\rangle$ on L. This is, from the analyst's point of view, the most probable sensor-determined penetrator position at the time t_0.

From now on, the "hat symbol" (^) will be used to indicate sensor-determined or sensor-dependent values, as distinct from maneuver-induced values to be introduced later. The ^-values are conditional. The condition is "no maneuver." The "bracket symbol" (< >) will always carry the meaning "most probable from the analyst's point of view."

In principle, the penetrator has six degrees-of-freedom -- three in position and three in velocity. At the outset, however, we assume that the penetrator always flies within a horizontal plane, thus eliminating one velocity degree-of-freedom. This assumption is generally valid except near the target. Each penetrator now has five degrees-of-freedom, where the velocity is now represented by the penetrator speed v and heading ψ. (Heading will always be taken from north, as in figure 3.)

The point $\langle\hat{P}(t_0)\rangle$ on the expected path L must be "suitably selected." In fact, the coordinates of $\langle\hat{P}(t_0)\rangle$, i.e., $[\langle\hat{x}(t_0)\rangle, \langle y(t_0)\rangle]$, are both functions of past maneuvers insofar as these maneuvers reduce the "effective speed" of the penetrator along its expected path. In essence, then, we model maneuver capability in part through the calculation of $\langle\hat{P}(t_0)\rangle$. Better, we model maneuver capability by treating it as a perturbation of the penetrator's movement along its expected path. This is the essence of the "perturbation approach."

Connected to the most probable observed penetrator position $\langle\hat{P}(t_0)\rangle$ is the most probable observed velocity $\langle\hat{\vec{v}}\rangle$ which is shown in figure 3. We decompose this velocity into speed and heading. The most probable observed speed is $\langle\hat{v}\rangle$ which is just the operational, or cruising, speed of the penetrator. It is a fixed parameter; that is, it keeps the same value at all times. The most probable observed heading $\langle\hat{\psi}\rangle$ is just the heading characterizing the expected path L. Because L is straight, $\langle\hat{\psi}\rangle$ assumes the

same value along all points of L. Finally, we choose as the most probable observed penetrator altitude $\langle\hat{z}\rangle$, the operational, or cruising, penetrator altitude h.

The geometry of the perturbation approach is illustrated in figure 4, which focuses on that section of the expected penetrator trajectory L which contains the most probable position $\langle\hat{P}(t_o)\rangle$. The penetrator's freedom to maneuver is now accounted for by the "change-of-speed" $\overset{+}{v}$ and the "change of heading" $\overset{+}{\psi}$. From now on, the "plus symbol" (+) will be used to identify maneuver-induced or maneuver-dependent values.

It now follows that the "state of the penetrator" at the time t_o is described by seven distribution functions. These are $\hat{X}[\hat{x}(t_o)]$, $\hat{Y}[\hat{y}(t_o)]$, $\hat{Z}[\hat{z}, t_o]$, $\hat{V}[\hat{v}, t_o]$, $\overset{+}{V}[\overset{+}{v}]$, $\hat{\Psi}[\hat{\psi},t_o]$, and $\overset{+}{\Psi}[\overset{+}{\psi}]$. Here the arguments such as $\hat{x}(t_o)$ are the statistically contemplated values as distinct from the most probable, or expectation, values such as $\langle\hat{x}(t_o)\rangle$. For the distributions such as $\hat{Z}[\hat{z},t_o]$, the quantity $\hat{z}$ is time-independent, but the uncertainty in its measurement remains time-dependent because it depends on the penetrator position relative to the sensor. Thus, the distribution $\hat{Z}[\hat{z},t_o]$ is *time-dependent, as indicated by the notation.*

3. The Distribution Functions

a. Distribution of Measurables. Let us first enumerate the distribution functions pertaining to measured quantities. We take the position distribution functions (PDFs) of $\hat{x}(t_o)$ and $\hat{y}(t_o)$ to be Gaussian[1]:

$$\hat{X}[\hat{x}(t_o)] = \frac{1}{\hat{\sigma}_x(t_o)\sqrt{2\pi}} \exp\left\{-\frac{[\hat{x}(t_o)-\langle\hat{x}(t_o)\rangle]^2}{2\hat{\sigma}_x^2(t_o)}\right\} \qquad (1)$$

$$\hat{Y}[\hat{y}(t_o)] = \frac{1}{\hat{\sigma}_y(t_o)\sqrt{2\pi}} \exp\left\{-\frac{[\hat{y}(t_o)-\langle\hat{y}(t_o)\rangle]^2}{2\hat{\sigma}_y^2(t_o)}\right\} \qquad (2)$$

---

1. The implications of doing so are explained in D.C. Baird, Experimentation: An Introduction to Measurement Theory and Experimental Design, Prentice-Hall, Inc., Englewood Cliffs, New Jersey, 1962, pp. 6-45. (Short Title - Baird)

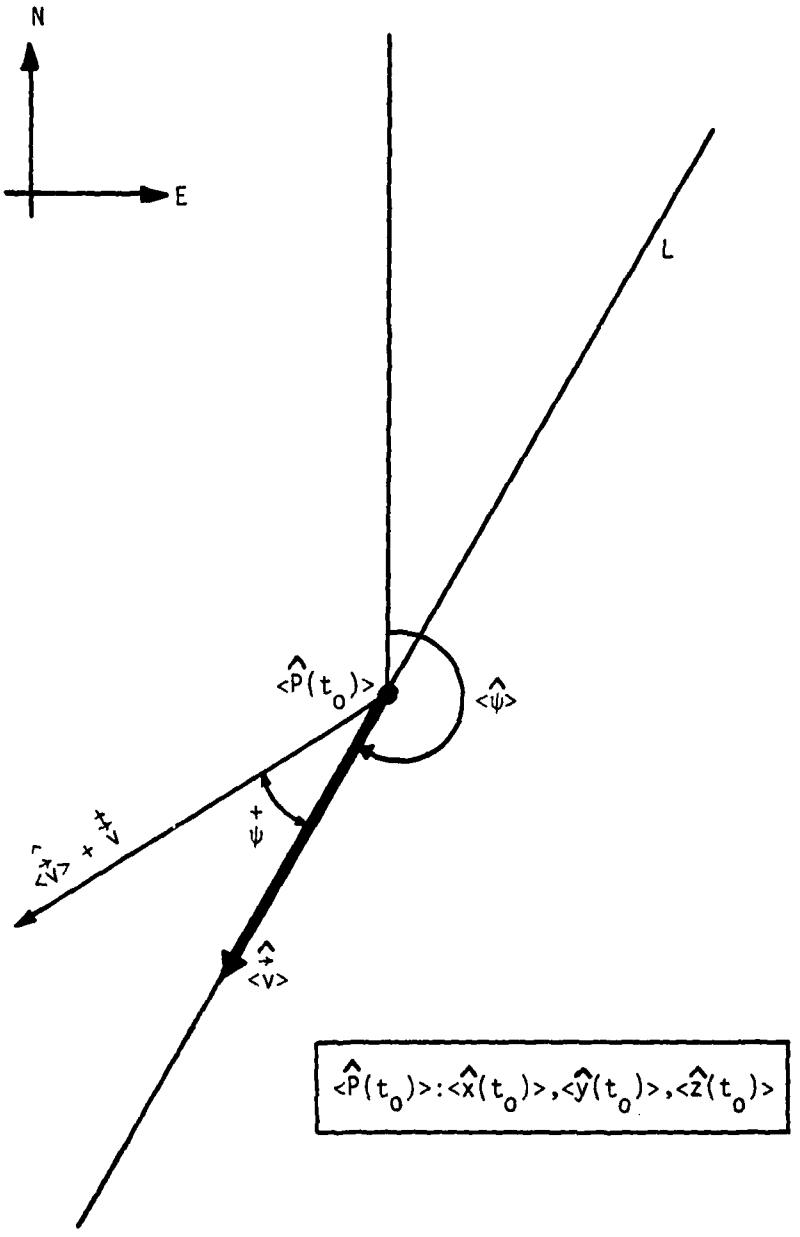

Figure 4. Geometry of the Perturbation Approach

We take a truncated Gaussian for $\hat{Z}[\hat{z}, t_o]$. The truncation simulates the fact that the sensor never indicates the penetrator is at or below ground level. Renormalization then yields[1]

$$\hat{Z}[\hat{z},t_o] = \frac{1}{\hat{\sigma}_z^*(t_o)\sqrt{2\pi}} \exp\left\{-\frac{[\hat{z}-\langle\hat{z}\rangle]^2}{2\hat{\sigma}_z^2(t_o)}\right\} \tag{3a}$$

$$\tilde{\sigma}_z^* \equiv \hat{\sigma}_z\, Q(-\langle\hat{z}\rangle/\hat{\sigma}_z) \tag{3b}$$

$$Q(-\langle\hat{z}\rangle/\hat{\sigma}_z) \equiv \frac{1}{\hat{\sigma}_z\sqrt{2\pi}} \int_0^{+\infty} \exp\left\{-\frac{[\hat{z}-\langle\hat{z}\rangle]^2}{2\hat{\sigma}_z^2}\right\} d\hat{z} \tag{3c}$$

We also take a Gaussian for the speed distribution function (SDF) of $\hat{v}$:

$$\hat{V}[\hat{v},t_o] = \frac{1}{\hat{\sigma}_v(t_o)\sqrt{2\pi}} \exp\left\{-\frac{[\hat{v}-\langle\hat{v}\rangle]^2}{2\hat{\sigma}_v^2(t_o)}\right\} \tag{4}$$

The heading distribution function (HDF) of $\hat{\psi}$ should reflect the property that the raid enters the defended area from a most favored direction. To account for this, we take a Gaussian in tan $\hat{\psi}$:

$$\hat{\Psi}[\tan\hat{\psi},t_o] = \frac{1}{\hat{\sigma}_\psi(t_o)\sqrt{2\pi}} \exp\left\{-\frac{[\tan\hat{\psi}-\tan\langle\hat{\psi}\rangle]^2}{2\hat{\sigma}_\psi^2(t_o)}\right\} \tag{5}$$

---

1. The Gaussian probability function $Q(x)$ is tabulated in M. A. Abramowitz and I.A. Stegun, Handbook of Mathematical Functions, National Bureau of Standards, Washington DC, 1965, pp. 931-932, 966-972; see also equation (26.2.19). (Short title - A&S)

The assumed HDF is designed to disallow headings in the interval $-\frac{\pi}{2} \leq \hat{\psi} \leq \frac{\pi}{2}$. Equation (5) also includes the implicit approximation $\langle \tan\hat{\psi} \rangle \simeq \tan\langle \hat{\psi} \rangle$ which is accurate for $\langle \hat{\psi} \rangle \simeq 0$, but also for $\langle \hat{\psi} \rangle \simeq \pi$.

b. Distribution of Maneuvers. Let us now enumerate the distribution functions pertaining to maneuver-induced quantities. We first note that these are likely to be symmetric; that is, the penetrator is equally likely to change to a more westerly heading as to a more easterly one, and it is equally likely to slow down as to speed up. These considerations suggest to account for maneuvers by using Gaussians with the corresponding expectation values set to zero. We therefore select for the change-of-speed distribution function (CSDF)

$$\overset{+}{V}[\overset{+}{v}] = \frac{1}{\overset{+}{\sigma}_v \sqrt{2\pi}} \exp\left\{ \frac{-[\overset{+}{v} - \langle \overset{+}{v} \rangle]^2}{2\overset{+2}{\sigma}_v} \right\} \tag{6a}$$

$$\langle \overset{+}{v} \rangle = 0 \tag{6b}$$

and for the change-of-heading distribution function (CHDF)

$$\overset{+}{\Psi}[\tan\overset{+}{\psi}] = \frac{1}{\overset{+}{\sigma}_\psi \sqrt{2\pi}} \exp\left\{ - \frac{[\tan\overset{+}{\psi} - \langle \tan\overset{+}{\psi} \rangle]^2}{2\overset{+2}{\sigma}_\psi} \right\} \tag{7a}$$

$$\langle \tan\overset{+}{\psi} \rangle = 0 \tag{7b}$$

The CHDF also simulates the most favored direction property. In addition, we take $\overset{+}{\sigma}_\psi$ and $\overset{+}{\sigma}_v$ to be independent of one another and to be constant over the entire expected path L.

4. Expectation Values and Standard Deviations. Our enumeration of the distribution functions is incomplete without an estimate of the expectation values $\langle \hat{x}(t_0) \rangle$, $\langle \hat{y}(t_0) \rangle$, and the maneuver-induced standard deviations $\overset{+}{\sigma}_v$, $\overset{+}{\sigma}_\psi$. Let us first show how to determine $\langle \hat{x}(t_0) \rangle$, $\langle \hat{y}(t_0) \rangle$.

a. Expectation Values. The expectation values of the penetrator position coordinates will be calculated from the equations

$$\langle \hat{x}(t_o) \rangle = x_F + v_e \sin\langle \hat{\psi} \rangle \, (t_o - t_F) \tag{8}$$

$$\langle \hat{y}(t_o) \rangle = y_F + v_e \cos\langle \hat{\psi} \rangle \, (t_o - t_F) \tag{9}$$

which follow from figure 4. In these equations, v_e is the "effective penetrator speed along L". Even though the most probable sensor-observed penetrator velocity $\langle \hat{\vec{v}} \rangle$ lies along L, its magnitude is not the effective penetrator speed along L; that is, $\langle \hat{v} \rangle \geq v_e$. This is a maneuver effect which has the consequence that v_e is the root-mean-square of $\langle \hat{v} \rangle \cos\overset{+}{\psi}$; that is,

$$\begin{aligned} v_e^2 &= \frac{\langle \hat{v} \rangle^2}{\overset{+}{\sigma}_\psi \sqrt{2\pi}} \int_{-\infty}^{+\infty} \cos^2 \overset{+}{\psi} \exp\left(\frac{-\tan^2 \overset{+}{\psi}}{2\overset{+2}{\sigma}_\psi}\right) d(\tan \overset{+}{\psi}) \\ &= \frac{\langle \hat{v} \rangle^2}{\overset{+}{\sigma}_\psi \sqrt{2\pi}} \int_{-\infty}^{+\infty} \frac{\exp(-\overset{+2}{\mu}/2\overset{+2}{\sigma}_\psi)}{1 + \overset{+2}{\mu}} \, d\overset{+}{\mu} \end{aligned} \tag{10}$$

The integral has a closed-form solution[1]; we find

$$v_e^2 = \left\{ \sqrt{\frac{\pi}{2}} \; \frac{\exp(1/2\overset{+2}{\sigma}_\psi)}{\overset{+}{\sigma}_\psi} \; \mathrm{erfc}(1/\overset{+}{\sigma}_\psi \sqrt{2}) \right\} \langle \hat{v} \rangle^2 \tag{11}$$

where erfc(x) is the complementary error function.[2]

---

1. A&S, equation (7.4.11), p. 302.

2. A tabulation of erfc(x) is given in A&S, pp. 297, 310-311; see also equation (7.1.28).

b. Standard Deviations

1. Maneuver-Induced Standard Deviations. We next turn to the maneuver-induced standard deviations $\overset{+}{\sigma}_{\psi}$ and $\overset{+}{\sigma}_{v}$. Even though we consider these parameters as freely selectable, we can estimate their values as functions of the penetrator range R_p. Figure 5 illustrates an extreme maneuver which takes the penetrator far away from the expected path L. In this case, the travel distance from P_F to P_T is 2a, and the total travel distance is subject to the restriction

$$R_{BF} + 2a + R_{TR} = R_P \tag{12}$$

from which

$$a = \frac{1}{2}(R_P - R_{BF} - R_{TR}) \tag{13}$$

Hence the angle ξ from figure 5 is

$$\xi = \arccos(R_{FT}/2a) \tag{14}$$

A reasonable estimate of $\overset{+}{\sigma}_{\psi}$ is then given by the equation

$$\overset{+}{\sigma}_{\psi} = \tan(\tfrac{1}{2}\xi) \tag{15}$$

Even though we take $\overset{+}{\sigma}_{\psi}$ and $\overset{+}{\sigma}_{v}$ to be independent, we can still derive a baseline value for $\overset{+}{\sigma}_{v}$ through practical considerations as follows. The generic scenario calls for simultaneous weapon detonations which means that a penetrator flying along the extreme path of figure 5 would have to move at increased speed. We therefore set

$$(\langle\hat{v}\rangle + \overset{+}{\sigma}_{v})(t_T - t_F) = 2a \tag{16}$$

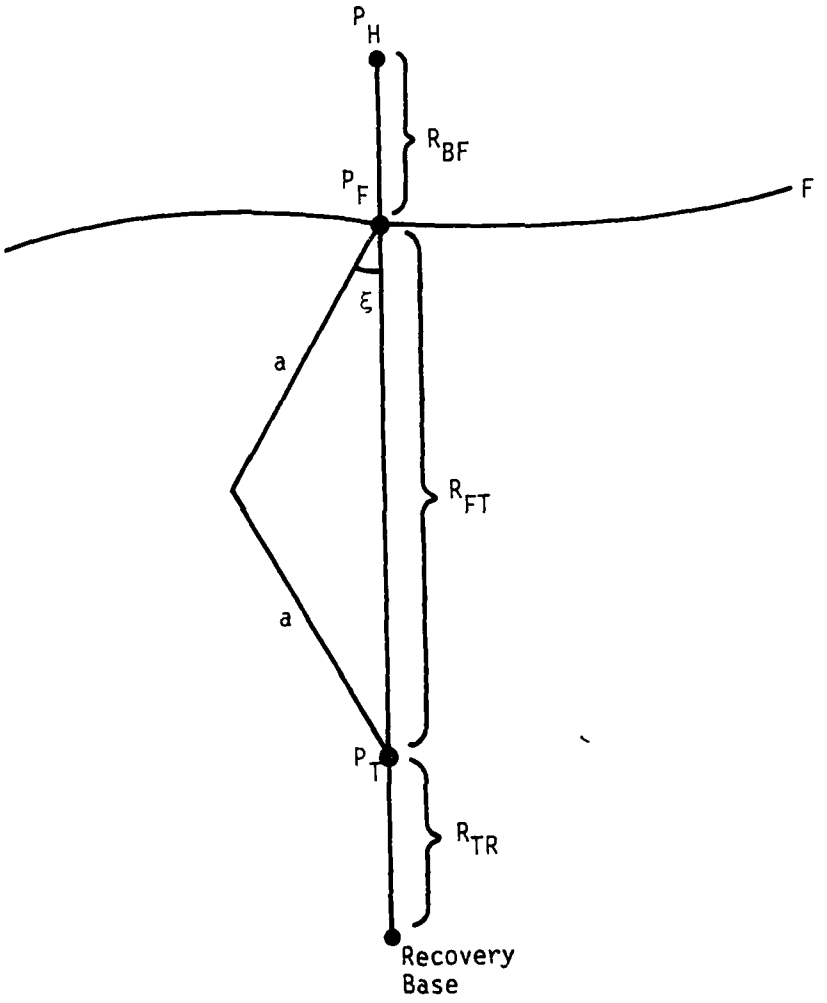

Figure 5. "Extreme Maneuver" - An Example

By the same logic, a penetrator which flies along the expected path L would have to travel at decreased speed. Hence we write

$$(\langle\hat{v}\rangle - \overset{+}{\sigma}_v)\,(t_T - t_F) = R_{FT} \tag{17}$$

The solution of these equations is

$$\overset{+}{\sigma}_v = \left(\frac{2a - R_{FT}}{2a + R_{FT}}\right)\langle\hat{v}\rangle \tag{18}$$

2. Sensor-Induced Standard Deviations. We begin with the observation that sensor-induced standard deviations are usually expressed in terms of down-range and cross-range position errors, and in terms of radial and tangential velocity errors. In other words, sensor errors are usually quoted relative to a spherical coordinate system with the origin at the sensor. Hence it is necessary to transform the standard deviations from sensor coordinates to air base coordinates. The details are explained in appendix A. The results are:

$$\begin{aligned}\hat{\sigma}_x^2(t_o) = {} & \sigma_R^2 \sin^2[\hat{\theta}(t_o)]\cos^2[\hat{\phi}(t_o)] + \\ & + [\sigma_{EL}\hat{r}_{SP}(t_o)]^2 \cos^2[\hat{\theta}(t_o)]\cos^2[\hat{\phi}(t_o)] + \\ & + [\sigma_{AZ}\,\hat{r}_{SP}(t_o)]^2\sin^2[\hat{\theta}(t_o)]\sin^2[\hat{\phi}(t_o)]\end{aligned} \tag{19a}$$

$$\begin{aligned}\hat{\sigma}_y^2(t_o) = {} & \sigma_R^2 \sin^2[\hat{\theta}(t_o)]\sin^2[\hat{\phi}(t_o)] + \\ & + [\sigma_{EL}\hat{r}_{SP}(t_o)]^2\cos^2[\hat{\theta}(t_o)]\sin^2[\hat{\phi}(t_o)] + \\ & + [\sigma_{AZ}\,\hat{r}_{SP}(t_o)]^2\sin^2[\hat{\theta}(t_o)]\cos^2[\hat{\phi}(t_o)]\end{aligned} \tag{19b}$$

$$\hat{\sigma}_z^2(t_o) = \sigma_R^2 \cos^2[\hat{\theta}(t_o)] + [\sigma_{EL}\hat{r}_{SP}(t_o)]^2 \sin^2[\hat{\theta}(t_o)] \quad (19c)$$

$$\hat{\sigma}_v^2(t_o) = \sigma_{vR}^2 \sin^2[\hat{\theta}(t_o)] \sin^2[\hat{\psi} + \hat{\phi}(t_o)] +$$
$$+ \sigma_{vEL}^2 \cos^2[\hat{\theta}(t_o)] \sin^2[\hat{\psi} + \hat{\phi}(t_o)] + \sigma_{vAZ}^2 \cos^2[\hat{\psi} + \hat{\phi}(t_o)] \quad (20a)$$

$$\hat{\sigma}_\psi^2(t_o) = \Big\{\sigma_{vR}^2 \sin^2[\hat{\theta}(t_o)] \cos^2[\hat{\psi} + \hat{\phi}(t_o)] +$$
$$+ \sigma_{vEL}^2 \cos^2[\hat{\theta}(t_o)] \cos^2[\hat{\psi} + \hat{\phi}(t_o)] +$$
$$+ \sigma_{vAZ}^2 \sin^2[\hat{\psi} + \hat{\phi}(t_o)]\Big\} \Big/ (\hat{v} \cos^2\hat{\psi})^2 \quad (20b)$$

$$\hat{\theta}(t_o) = \arcsin\left\{\frac{\sqrt{[x_{BP}(t_o) - x_{BS}(t_o)]^2 + [y_{BP}(t_o) - y_{BS}(t_o)]^2}}{\hat{r}_{SP}(t_o)}\right\} \quad (21a)$$

$$\hat{\phi}(t_o) = \arcsin\left\{\frac{y_{BP}(t_o) - y_{BS}(t_o)}{\sqrt{[x_{BP}(t_o) - x_{BS}(t_o)]^2 + [y_{BP}(t_o) - y_{BS}(t_o)]^2}}\right\} \quad (21b)$$

In these equations, σ_R is the range error, σ_{EL} is the elevation error, σ_{AZ} is the azimuthal error, σ_{vR} is the radial velocity error, σ_{vEL} is the elevation velocity error, and σ_{vAZ} is the azimuthal velocity error. The "hat symbol" is not applied here because it is obvious that these parameters refer to the sensor. The quantity $r_{SP}(t_o)$ is the distance between the sensor and penetrator at time t_o, and the subscripts "BS" and "BP" stand for "base-to-sensor" and "base-to-penetrator". (See also figure A2 in appendix A.) The angles $\hat{\theta}(t_o)$, $\hat{\phi}(t_o)$ and the distances $\hat{r}_{SP}(t_o)$, $\hat{r}_{BP}(t_o)$ are obviously time-dependent, and $r_{BS}(t_o)$ is time-dependent, given a mobile sensor.

B. EVOLUTION OF THE POSITION DISTRIBUTION FUNCTIONS

We have seen how to characterize a sensor reading at arbitrary time t_o. This subsection will develop the PDFs at time $t>t_o$, given no additional sensor readings after time t_o. The solution lies in a series of convolutions.

Let us begin with the "total speed"

$$v = \hat{v} + \overset{+}{v} \tag{22}$$

which is described by the total speed distribution function (TSDF), V[v]. This function can be derived from the equation

$$V[v] = \int_{-\infty}^{+\infty} V[v|\overset{+}{v}]\ \overset{+}{V}[\overset{+}{v}]\ d\overset{+}{v} \tag{23}$$

where $V[v|\overset{+}{v}]$ is the "conditional TSDF". It satisfies the relation[1]

$$V[v|\overset{+}{v}]\ dv = \hat{V}[\hat{v}]\ d\hat{v} \tag{24}$$

Here, we observe equation (22) and the relation $dv=d\hat{v}$ which follows from equation (22) under the statistical condition $d\overset{+}{v} = 0$. This yields

$$V[v|\overset{+}{v}] = \hat{V}[v-\overset{+}{v}] \tag{25}$$

It then follows that the integral of equation (23) is the convolution of two Gaussians which has the solution

$$V[v, t_o] = \frac{1}{\sigma_v(t_o)\sqrt{2\pi}} \exp\left\{-\frac{[v-\langle v\rangle]^2}{2\sigma_v^2(t_o)}\right\} \tag{26a}$$

---

1. This technique for interchanging distribution functions is common; see for example F.S. Hillier and G.J. Lieberman, Operations Research, Holden Day, Inc., San Francisco, 1967, p. 347.

where

$$\sigma_v^2 (t_o) = \hat{\sigma}_v^2 (t_o) + \overset{+2}{\sigma}_v \tag{26b}$$

$$\langle v \rangle = \langle \hat{v} \rangle \tag{26c}$$

Using the same techniques, we can now calculate X[x(t)] and Y[y(t)]. (Our ignoring maneuvers in the z-direction is equivalent to setting $Z[z(t)] = Z[\hat{z}, t_o]$.) The formal solutions are

$$X[x(t)] = \int_{-\infty}^{+\infty} \int_{-\infty}^{+\infty} \int_{-\infty}^{+\infty} X[x'(t) | \hat{x}(t_o), \hat{\psi}, \overset{+}{\psi}] \; \hat{X}[\hat{x}(t_o)] \; x$$

$$x \; \hat{\Psi}[\tan\hat{\psi}, t_o] \; \overset{+}{\Psi} [\tan\overset{+}{\psi}] d[\hat{x}(t_o)] d(\tan\hat{\psi}) d(\tan\overset{+}{\psi}) \tag{27a}$$

$$Y[y(t)] = \int_{-\infty}^{+\infty} \int_{-\infty}^{+\infty} \int_{-\infty}^{+\infty} Y[y(t) | \hat{y}(t_o), \hat{\psi}, \overset{+}{\psi}] \; \hat{Y}[\hat{y}(t_o)] \; x$$

$$x \; \hat{\Psi}[\tan\hat{\psi}, t_o] \; \overset{+}{\Psi} [\tan \overset{+}{\psi}] \; d[\hat{y}(t_o)] \; d(\tan\hat{\psi}) \; d(\tan\overset{+}{\psi}) \tag{27b}$$

Here, we have

$$X[x(t) | \hat{x}(t_o), \hat{\psi}, \overset{+}{\psi}] |dx(t)| = V[v] |dv| \tag{28a}$$

$$Y[y(t) | \hat{y}(t_o), \hat{\psi}, \overset{+}{\psi}] |dy(t)| = V[v] |dv| \tag{28b}$$

These allow us to derive the conditional distribution functions on the left side. To this end, we first observe in analogy to equations (8) and (9) that

$$\langle x(t) \rangle = \langle \hat{x}(t_o) \rangle + v_e \sin\langle \hat{\psi} \rangle \; (t - t_o) \tag{29a}$$

$$\langle y(t) \rangle = \langle \hat{y}(t_o) \rangle + v_e \cos\langle \hat{\psi} \rangle \; (t - t_o) \tag{29b}$$

where v_e is the effective penetrator speed defined by equation (11). Since equations (29) contain only expectation values, in other words, temporal constants, they hold true for finite time intervals $(t-t_o)$. If we remove the bracket operators, we obtain

$$x(t) = \hat{x}(t_o) + v\, S(t-t_o) \tag{30a}$$

$$y(t) = \hat{y}(t_o) + v\, C(t-t_o) \tag{30b}$$

$$S \equiv \sin(\hat{\psi} + \overset{+}{\psi}) \tag{30c}$$

$$C \equiv \cos(\hat{\psi} + \overset{+}{\psi}) \tag{30d}$$

However, because of the statistical fluctuations of v, $\hat{\psi}$, and $\overset{+}{\psi}$, equations (30) hold true only for infinitesimally small time intervals $(t-t_o)$. On the other hand, if we proceed from x(t), y(t) to the statistical uncertainties dx(t), dy(t), the temporal condition no longer applies. If, at the same time, we observe the statistical constants listed in the condition compartments of equations (28), we obtain

$$dx(t) = (t-t_o)\, S\, dv \tag{31a}$$

$$dy(t) = (t-t_o)\, C\, dv \tag{31b}$$

We repeat that these are not temporal differentials, but rather these are statistical differentials.

If now equations (26), (29), (30), and (31) are inserted in equations (28), we obtain

$$X[x(t)|\hat{x}(t_o),\ \hat{\psi},\ \overset{+}{\psi}] =$$

$$= \frac{1}{(t-t_o)\ \sigma_v |S| \sqrt{2\pi}} \quad \exp\left\{ - \frac{[x(t) - \hat{x}(t_o) - S\rho(t)]^2}{2S^2 \sigma_v^2 (t-t_o)^2} \right\} \tag{32a}$$

$$Y[y(t)|\hat{y}(t_o),\hat{\psi},\overset{+}{\psi}] = \frac{1}{(t-t_o)\sigma_v|C|\sqrt{2\pi}} \exp\left\{-\frac{[y(t)-\hat{y}(t_o)-C\rho(t)]^2}{2C^2\sigma_v^2(t-t_o)^2}\right\} \quad (32b)$$

$$\rho(t) \equiv \frac{<x(t)> - <\hat{x}(t_o)>}{<S>} = \frac{<y(t)> - <\hat{y}(t_o)>}{<C>} = <v>(t-t_o) \quad (32c)$$

If next we insert equations (32), (1), and (2) into equations (27), we see immediately that the integrals over $\hat{x}(t_o)$ and $\hat{y}(t_o)$ are merely simple convolutions resulting in

$$X[x(t)|\hat{\psi}, \overset{+}{\psi}] = \frac{1}{\sigma_S(t)\sqrt{2\pi}} \exp\left\{-\frac{[x(t)-<\hat{x}(t_o)> - S\rho(t)]^2}{2\sigma_S^2(t)}\right\} \quad (33a)$$

$$Y[y(t)|\psi,\overset{+}{\psi}] = \frac{1}{\sigma_C(t)\sqrt{2\pi}} \exp\left\{-\frac{[y(t)-<\hat{y}(t_o)>-C\rho(t)]^2}{2\sigma_C^2(t)}\right\} \quad (33b)$$

$$\sigma_S^2(t) \equiv \hat{\sigma}_x^2(t_o) + S^2(t-t_o)^2\,\sigma_v^2(t) \quad (33c)$$

$$\sigma_C^2(t) \equiv \hat{\sigma}_y^2(t_o) + C^2(t-t_o)^2\,\sigma_v^2(t) \quad (33d)$$

For further treatment, we introduce the abbreviations

$$\hat{\mu} \equiv \tan\hat{\psi} \quad ; \quad \overset{+}{\mu} \equiv \tan\overset{+}{\psi} \quad (34a,b)$$

We then note that

$$S(\hat{\mu}, \overset{+}{\mu}) = \frac{\hat{\mu} + \overset{+}{\mu}}{\sqrt{(1+\hat{\mu}^2)(1+\overset{+}{\mu}^2)}} \; ; \quad C(\hat{\mu}, \overset{+}{\mu}) = \frac{1-\hat{\mu}\overset{+}{\mu}}{\sqrt{(1+\hat{\mu}^2)(1+\overset{+}{\mu}^2)}} \quad (35a,b)$$

Our problem now reduces to solving the following convolution integrals:

$$X[x(t)] = \int_{-\infty}^{+\infty}\int_{-\infty}^{+\infty} G_x(\hat{\mu},\overset{+}{\mu})\,\hat{\Psi}(\hat{\mu})\,\overset{+}{\Psi}(\overset{+}{\mu})\,d\hat{\mu}\,d\overset{+}{\mu} \quad (36a)$$

$$Y[y(t)] = \int_{-\infty}^{+\infty}\int_{-\infty}^{+\infty} G_y(\hat{\mu},\overset{+}{\mu})\ \hat{\Psi}(\hat{\mu})\ \overset{+}{\Psi}(\overset{+}{\mu})d\hat{\mu}\ d\overset{+}{\mu} \tag{36b}$$

$$G_x(\hat{\mu},\overset{+}{\mu}) \equiv \frac{1}{\sigma_S(\hat{\mu},\overset{+}{\mu})\ \sqrt{2\pi}}\quad \exp\left\{-\frac{[x(t) - <\hat{x}(t_o)> - S(\hat{\mu},\overset{+}{\mu})\rho(t)]^2}{2\sigma_S^2(\hat{\mu},\overset{+}{\mu})}\right\} \tag{36c}$$

$$G_y(\hat{\mu},\overset{+}{\mu}) \equiv \frac{1}{\sigma_C(\hat{\mu},\overset{+}{\mu})\ \sqrt{2\pi}}\quad \exp\left\{-\frac{[y(t) - <\hat{y}(t_o)> - C(\hat{\mu},\overset{+}{\mu})\rho(t)]^2}{2\sigma_C^2(\hat{\mu},\overset{+}{\mu})}\right\} \tag{36d}$$

These are not simple convolutions because G_x and G_y depend on $\hat{\mu}$ and $\overset{+}{\mu}$ in a "non-Gaussian" way. Nevertheless, the integrals can be solved approximately via an expansion about moments. As is shown in appendix B, the solutions to second order in $\hat{\sigma}_\psi$ and $\overset{+}{\sigma}_\psi$ are as follows:

$$X[x(t)] = G_x(<\hat{\psi}>,\ o)\ [1 + \sum_{i=o}^{4} X_i\ (\Delta x)^i] \tag{37a}$$

$$Y[y(t)] = G_y(<\hat{\psi}>, o)\ [1 + \sum_{i=o}^{4} Y_i (\Delta y)^i] \tag{37b}$$

$$\Delta x \equiv x(t) - <\hat{x}(t_o)> - \rho(t)\ \sin\ <\hat{\psi}> \tag{37c}$$

$$\Delta y \equiv y(t) - <\hat{y}(t_o)> - \rho(t)\ \cos<\hat{\psi}> \tag{37d}$$

$$X_i = \tfrac{1}{2}\ \sigma_S\ \sqrt{2\pi}\ \ (\hat{\sigma}_\psi^2 \hat{X}_i + \overset{+}{\sigma}_\psi^2 \overset{+}{X}_i) \tag{37d}$$

$$Y_i = \tfrac{1}{2}\ \sigma_C\ \sqrt{2\pi}\ \ (\hat{\sigma}_\psi^2 \hat{Y}_i + \overset{+}{\sigma}_\psi^2 \overset{+}{Y}_i) \tag{37f}$$

$$\hat{X}_4 = \frac{\sigma_v^4 (t-t_o)^4 \sin^2(2\langle\hat{\psi}\rangle) \cos^4\langle\hat{\psi}\rangle}{4\sigma_S^9 \sqrt{2\pi}} \tag{37g}$$

$$\hat{X}_3 = \frac{\sigma_v^2(t-t_o)^2 \cos^5\langle\hat{\psi}\rangle \sin(2\langle\hat{\psi}\rangle)}{\sigma_S^7 \sqrt{2\pi}} \tag{37h}$$

$$\hat{X}_2 = \frac{\sigma_v^2(t-t_o)^2 \cos^4\langle\hat{\psi}\rangle(1-4\sin^2\langle\hat{\psi}\rangle) + \rho^2 \cos^6\langle\psi\rangle}{\sigma_S^5 \sqrt{2\pi}} - 6\sigma_S^2 \hat{X}_4 \tag{37i}$$

$$\hat{X}_1 = -3\rho \sin\langle\hat{\psi}\rangle \cos^4\langle\hat{\psi}\rangle \left[\frac{\sigma_S^2 + 2\sigma_v^2(t-t_o)^2 \cos^2\langle\hat{\psi}\rangle}{\sigma_S^5 \sqrt{2\pi}}\right] \tag{37j}$$

$$\hat{X}_o = -\sigma_S^2(3\sigma_S^2 \hat{X}_4 + \hat{X}_2) \tag{37k}$$

$$\overset{+}{X}_4 = \frac{\sigma_v^4(t-t_o)^4 \sin^2(2\langle\hat{\psi}\rangle)}{4\sigma_S^9 \sqrt{2\pi}} \tag{37l}$$

$$\overset{+}{X}_3 = \frac{\sigma_v^2 (t-t_o)^2 \rho\cos\langle\hat{\psi}\rangle \sin(2\langle\hat{\psi}\rangle)}{\sigma_S^7 \sqrt{2\pi}} \tag{37m}$$

$$\overset{+}{X}_2 = \frac{\sigma_v^2 (t-t_o)^2 \cos(2\langle\hat{\psi}\rangle) + \rho^2 \cos^2\langle\hat{\psi}\rangle}{\sigma_S^5 \sqrt{2\pi}} - 6\sigma_S^2 \overset{+}{X}_4 \tag{37n}$$

$$\overset{+}{X}_1 = -\rho \sin\langle\hat{\psi}\rangle \left[\frac{\sigma_S^2 + 6\sigma_v^2 (t-t_o)^2 \cos^2\langle\hat{\psi}\rangle}{\sigma_S^5 \sqrt{2\pi}}\right] \tag{37o}$$

$$\overset{+}{X}_o = -\sigma_S^2 (3\sigma_S^2 \overset{+}{X}_4 + \overset{+}{X}_2) \tag{37p}$$

$$\hat{Y}_4 = \frac{\sigma_v^4 (t-t_o)^4 \sin^2(2\langle\hat{\psi}\rangle) \cos^4\langle\hat{\psi}\rangle}{4\sigma_C^9 \sqrt{2\pi}} \tag{37q}$$

$$\hat{Y}_3 = \frac{\sigma_v^2 (t-t_o)^2 \rho \sin^2(2\langle\hat{\psi}\rangle) \cos^3\langle\hat{\psi}\rangle}{2\sigma_C^7 \sqrt{2\pi}} \tag{37r}$$

$$\hat{Y}_2 = \frac{\sigma_v^2 (t-t_o)^2 \cos^4\langle\hat{\psi}\rangle (4\sin^2\langle\hat{\psi}\rangle - 1) + \rho^2 \sin^2\langle\hat{\psi}\rangle \cos^4\langle\hat{\psi}\rangle}{\sigma_C^5 \sqrt{2\pi}} - 6\sigma_C^2 \hat{Y}_4 \tag{37s}$$

$$\hat{Y}_1 = \rho \cos^3\langle\hat{\psi}\rangle \left[\frac{(3\sin^2\langle\hat{\psi}\rangle - 1)\sigma_C^2 - 6\sigma_v^2 (t-t_o)^2 \sin^2\langle\hat{\psi}\rangle \cos^2\langle\hat{\psi}\rangle}{\sigma_C^5 \sqrt{2\pi}}\right] \tag{37t}$$

$$\hat{Y}_o = -\sigma_C^2 (3\sigma_C^2 \hat{Y}_4 + \hat{Y}_2) \tag{37u}$$

$$\overset{+}{Y}_4 = \frac{\sigma_v^4 (t-t_o)^4 \sin^2(2\langle\hat{\psi}\rangle)}{4\sigma_C^9 \sqrt{2\pi}} \tag{37v}$$

$$\overset{+}{Y}_3 = \frac{\sigma_v^2 (t-t_o)^2 \rho \sin\langle\hat{\psi}\rangle \sin(2\langle\hat{\psi}\rangle)}{\sigma_C^7 \sqrt{2\pi}} \tag{37w}$$

$$\overset{+}{Y}_2 = \frac{\rho^2 \sin^2\langle\hat{\psi}\rangle - \sigma_v^2 (t-t_o)^2 \cos(2\langle\hat{\psi}\rangle)}{\sigma_C^5 \sqrt{2\pi}} - 6\sigma_C^2 \overset{+}{Y}_4 \tag{37x}$$

$$\overset{+}{Y}_1 = -\rho \cos\langle\hat{\psi}\rangle \left[\frac{\sigma_C^2 + 6\sigma_v^2 (t-t_o)^2 \sin^2\langle\hat{\psi}\rangle}{\sigma_C^5 \sqrt{2\pi}}\right] \tag{37y}$$

$$\overset{+}{Y}_o = -\sigma_C^2 (3\sigma_C^2 \overset{+}{Y}_4 + \overset{+}{Y}_2) \tag{37z}$$

In applying equations (37), we must remember that now

$$\sigma_S^2\ (t) = \hat{\sigma}_x^2\ (t_o) + \sin^2\langle\hat{\psi}\rangle\ \sigma_v^2(t)\ (t-t_o)^2 \tag{37aa}$$

$$\sigma_C^2\ (t) = \hat{\sigma}_y^2\ (t_o) + \cos^2\langle\hat{\psi}\rangle\ \sigma_v^2(t)\ (t-t_o)^2 \tag{37ab}$$

C. MORE ON THE POSITION DISTRIBUTION FUNCTIONS

The expansion presented by equations (37) is accurate for $\rho\sigma_\psi << \sigma_S$ and $\rho\sigma_\psi << \sigma_C$. Thus it has limited use in its present form. However, if we think about the kinematics of the problem, we can use the expansion to "back into" a more useful approximate solution.

Figure 6 shows how heading uncertainty enters the problem. The uncertainty induces a contribution $\rho\ \sin(\tan^{-1}\sigma_\psi)$ to the x-axis of the error basket, and a contribution $\rho[1-\cos(\tan^{-1}\sigma_\psi)]$ to the y-axis of the error basket. These extend σ_x and σ_y roughly in the conventional way:

$$\sigma_{x\ TOT}^2 \sim \sigma_S^2 + \rho^2\ \sin^2(\tan^{-1}\sigma_\psi) \tag{38a}$$

$$\sigma_{y\ TOT}^2 \sim \sigma_C^2 + \rho^2\ [1 - \cos(\tan^{-1}\sigma_\psi)]^2 \tag{38b}$$

Since we are treating cases for which $\sigma_\psi << 1$, we note that

$$\sin(\tan^{-1}\sigma_\psi) \simeq \sigma_\psi \tag{39a}$$

$$\cos(\tan^{-1}\sigma_\psi) \simeq \frac{1}{2}\ \sigma_\psi^2 \tag{39b}$$

Furthermore, when $\sigma_\psi << 1$, the error basket will continue to look roughly like a Gaussian ellipsoid over its entire evolution. Thus, we are led to expect solutions of the form

$$X[x(t)] \sim \frac{1}{\sqrt{2\pi\ (\sigma_S^2 + M\ \cos^2\langle\hat{\psi}\rangle\rho^2\ \sigma_\psi^2)}}\ \exp\left[\frac{-(\Delta x)^2}{2(\sigma_S^2 + M\ \cos^2\langle\hat{\psi}\rangle\rho^2\ \sigma_\psi^2)}\right] \tag{40a}$$

$$Y[y(t)] \sim \frac{1}{\sqrt{2\pi\left[\sigma_C^2 + N \sin^2\langle\hat{\psi}\rangle \rho^2 \sigma_\psi^2 + O(\rho^2 \sigma_\psi^4)\right]}} \times$$

$$\times \exp\left[\frac{-(\Delta y)^2}{2(\sigma_C^2 + N \sin^2\langle\hat{\psi}\rangle \rho^2 \sigma_\psi^2 + O(\rho^2 \sigma_\psi^4))}\right] \qquad (40b)$$

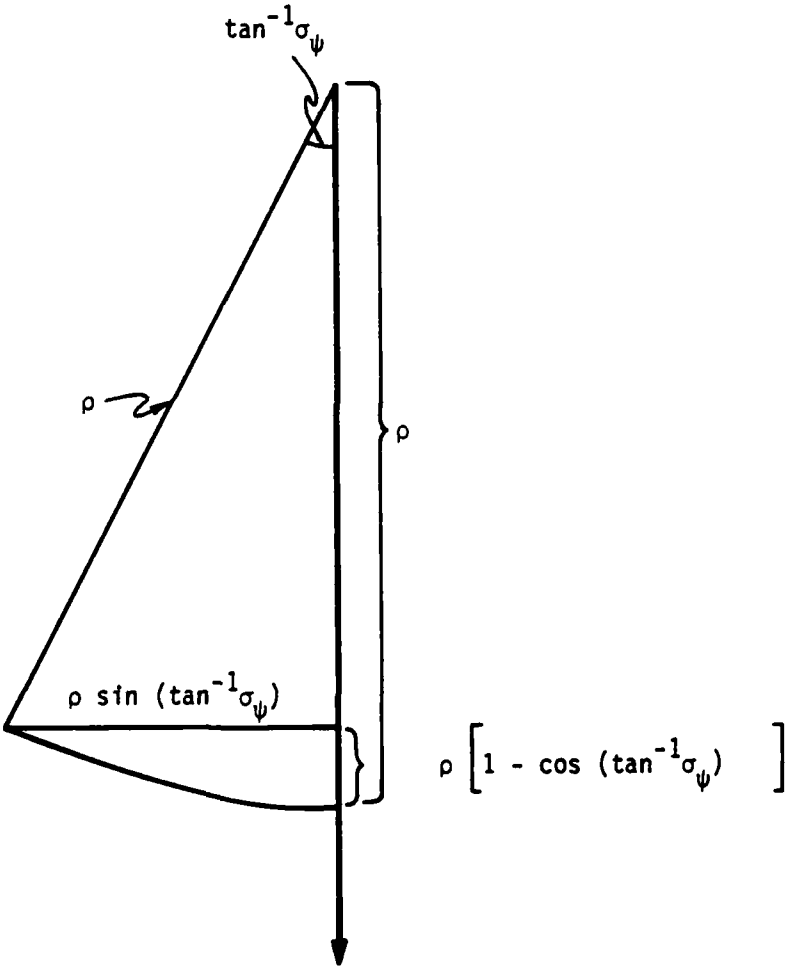

Figure 6. Effect of Heading Standard Deviation

We can now turn to the mathematics; i.e, the expansion, to find out what M, N are.

When we go to equations (37), we can first note that X_4, Y_4 are both always small. If we next observe that for most interesting problems $\sigma_v(t-t_o)<<\rho$, we can then note that X_3, Y_3 are generally small compared to X_2, Y_2, and we set

$$\hat{X}_2 \simeq \frac{\rho^2 \cos^6 <\hat{\psi}>}{\sigma_S^5 \sqrt{2\pi}} \tag{41a}$$

$$\overset{+}{X}_2 \simeq \frac{\rho^2 \cos^2 <\hat{\psi}>}{\sigma_S^5 \sqrt{2\pi}} \tag{41b}$$

$$\hat{Y}_2 \simeq \frac{\rho^2 \sin^2 <\hat{\psi}> \cos^4 <\hat{\psi}>}{\sigma_C^5 \sqrt{2\pi}} \tag{41c}$$

$$\overset{+}{Y}_2 \simeq \frac{\rho^2 \sin^2 <\hat{\psi}>}{\sigma_C^5 \sqrt{2\pi}} \tag{41d}$$

$$\hat{X}_1 \simeq \frac{-3\rho \sin <\hat{\psi}> \cos^4 <\hat{\psi}>}{\sigma_S^3 \sqrt{2\pi}} \tag{41e}$$

$$\overset{+}{X}_1 \simeq \frac{-\rho \sin <\hat{\psi}>}{\sigma_S^3 \sqrt{2\pi}} \tag{41f}$$

$$\hat{Y}_1 \simeq \frac{\rho \cos^3 <\hat{\psi}> (3\sin^2 <\hat{\psi}> - 1)}{\sigma_C^3 \sqrt{2\pi}} \tag{41g}$$

$$\overset{+}{Y}_1 \simeq \frac{-\rho \cos <\hat{\psi}>}{\sigma_C^3 \sqrt{2\pi}} \tag{41h}$$

$$\hat{X}_o \simeq - \sigma_S^2 \hat{X}_2 \tag{41i}$$

$$\overset{+}{X}_o \simeq - \sigma_S^2 \overset{+}{X}_2 \tag{41j}$$

$$\hat{Y}_o \simeq - \sigma_C^2 \hat{Y}_2 \tag{41k}$$

$$\overset{+}{Y}_o \simeq - \sigma_C^2 \overset{+}{Y}_2 \tag{41l}$$

Next, we expand in a Taylor series a Gaussian of the form

$$G(\Delta x) = \frac{1}{\sqrt{2\pi\sigma_S^2 + K\delta^2}} \quad \exp\left[\frac{-(\Delta x)^2}{2(\sigma_S^2 + K\delta^2)}\right] \tag{42}$$

with the result

$$G(\Delta x) \simeq \frac{1}{\sqrt{2\pi}\,\sigma_S} \exp\left[\frac{-(\Delta x)^2}{2\sigma_S^2}\right] + \frac{K}{2\sqrt{2\pi}}\left[\frac{(\Delta x)^2}{\sigma_S^5} - \frac{1}{\sigma_S^3}\right] \exp\left[\frac{-(\Delta x)^2}{2\sigma_S^2}\right] \tag{43a}$$

or, more simply,

$$G(\Delta x) \simeq G\left\{\left[1 - \frac{K}{2\sigma_S^2}\right] + \frac{(\Delta x)^2 K}{2\sigma_S^4}\right\} \tag{43b}$$

where G is the "unperturbed" Gaussian. We now write this in the more suggestive form

$$G(\Delta x) \simeq G\left\{1 - \sigma_S^2 X_2 + (\Delta x)^2 X_2\right\} \tag{43c}$$

With the help of equations (37e), (41a), (41b), this leads us to the identification

$$K\delta^2 = \rho^2 \cos^2\langle\hat{\psi}\rangle \, (\hat{\sigma}_\psi^2 \cos^4\langle\hat{\psi}\rangle + \hat{\sigma}_\psi^2) \tag{44}$$

We therefore reach the inductive conclusion

$$X[x(t)] \simeq \frac{1}{\sigma_X \sqrt{2\pi}} \exp\left[\frac{-(\Delta x)^2}{2\sigma_X^2}\right] + X_1 \, G_x(\langle\hat{\psi}\rangle, 0)\Delta x \tag{45a}$$

$$\sigma_X^2 \equiv \sigma_S^2 + \rho^2 \cos^2\langle\hat{\psi}\rangle \, (\sigma_\psi^2 \cos^4\langle\hat{\psi}\rangle + \hat{\sigma}_\psi^2) \tag{45b}$$

In exactly the same way, we conclude

$$Y[y(t)] \simeq \frac{1}{\sigma_Y \sqrt{2\pi}} \exp\left[-\frac{(\Delta y)^2}{2\sigma_Y^2}\right] + Y_1 G_y(\langle\hat{\psi}\rangle, 0)\, \Delta y \tag{45c}$$

$$\sigma_Y^2 \equiv \sigma_C^2 + \rho^2 \sin^2\langle\hat{\psi}\rangle \, (\hat{\sigma}_\psi^2 \cos^4\langle\hat{\psi}\rangle + \hat{\sigma}_\psi^2) \tag{45d}$$

We could go one step further and incorporate the X_1, Y_1 terms. If we did, they would impact the Gaussian through small additive terms, of order $\rho\sigma_\psi^2$, to Δx and Δy. Hence, we write instead

$$X[x(t)] \simeq \frac{1}{\sigma_X \sqrt{2\pi}} \exp\left[\frac{-(\Delta x)^2}{2\sigma_X^2}\right] \tag{46a}$$

$$Y[y(t)] \simeq \frac{1}{\sigma_Y \sqrt{2\pi}} \exp\left[\frac{-(\Delta y)^2}{2\sigma_Y^2}\right] \tag{46b}$$

These expressions are accurate for $\sigma_\psi \ll 1$, and for $\rho\sigma_\psi^2 \ll \sigma_X$, $\rho\sigma_\psi^2 \ll \sigma_Y$.

D. THE EXPECTED PROBABILITY OF KILL

Let P_K denote the conventional kill probability. This is a conditional probability, for it depends on the following:

1. The probability that the sensor successfully detects and tracks the penetrator (successful vectoring).

2. The probability that the interceptor's on-board sensor detects the penetrator (successful handover).

3. The probability that the weapon launched by the interceptor successfully homes on the penetrator, given penetrator detection (successful homing).

4. The probability that the weapon kills the interceptor, given that it homes (successful kill).

In the present paper, we do not address the problem of assessing these probabilities, but rather we consider them as inputs. More precisely, we assume that all of the probabilities mentioned above are consolidated in the probability

$$P_K = P_K [x_A, y_A, z_A, t_A \mid x(t_A), y(t_A), z(t_A)] \tag{47}$$

This is the probability that the weapon which is launched from the "attack position" (x_A,y_A,z_A) at the "attack time" t_A will kill the penetrator, given that the penetrator, at the attack time t_A, occupies the position $[x(t_A), y(t_A),z(t_A)]$. The present paper focuses on the probability that the penetrator will satisfy this condition. This probability is described by the position distribution functions $X[x(t_A)]$ and so forth. With the aid of these functions, we then calculate the "expected probability of kill"

$$\langle P_K(x_A,y_A,z_A,t_A)\rangle = \int_{-\infty}^{+\infty}\int_{-\infty}^{+\infty}\int_{-\infty}^{+\infty} P_K[x_A,y_A,z_A,t_A \mid x(t_A), y(t_A), z(t_A)]\, X[x(t_A)]\, Y[y(t_A)]\, Z[z(t_A)]\, dx(t_A)\, dy(t_A)\, dz(t_A) \tag{48}$$

Here we recall that this approach accounts for both sensor errors and maneuver effects.

III. THE BASIC ATTACK EQUATIONS

Any air intercept problem is driven by velocity and geometry considerations. By assumption, the geometry of our problem is euclidean; consequently, intercept is quantifiable using elementary vector analysis techniques, with the resulting solution depending largely on penetrator and interceptor velocities. This section develops the vector analysis tools required to calculate attack positions and attack times by focusing on one interceptor successively engaging several penetrators. For this purpose, penetrator maneuvers are ignored; their effect is the subject of section IV. This section begins with the intercept geometry, then turns to the impact of varied interceptor flight profiles, and finishes by "devectorizing" the attack equations for computerization.

A. INTERCEPT GEOMETRY

The basic intercept problem in which one interceptor successively attacks several non-maneuvering penetrators at close range is elementary. Figure 7 shows an overhead view of the intercept geometry. At time t_ℓ, the interceptor leaves point A* at which it previously attacked another penetrator. It flies with velocity $\vec{v}_I$ along the transit vector $\vec{T}_I$ to attack the present penetrator at the attack point A, and it arrives at A at time t_a. In general, attack takes place at a time $t_A > t_a$. For example, if the penetrator raid is tenuous, the interceptor may have to loiter for a time τ_L while awaiting the penetrator's arrival at A; and it generally will have to search for a time τ_S, depending on the performance of the fire control system. At the same time t_ℓ at which the interceptor leaves point A*, the penetrator leaves point Q and flies with velocity $\vec{v}$ along the transit vector $\vec{T}$ to point A where it is attacked at time t_A. The points Q, A*, and A are represented by vectors $\vec{r}_Q(t_\ell)$, $\vec{r}_A{}^*$, and $\vec{r}_A$, respectively. In addition, the C^3 network may carry a dead time τ_d for data processing and handover. Let us assume that the vectoring information is always internally adjusted for the dead time before handover; then its only impact is on the PDFs through equations (37). These considerations give rise to the following equations:

$$t_A = t_a + \tau_L + \tau_S \tag{49}$$

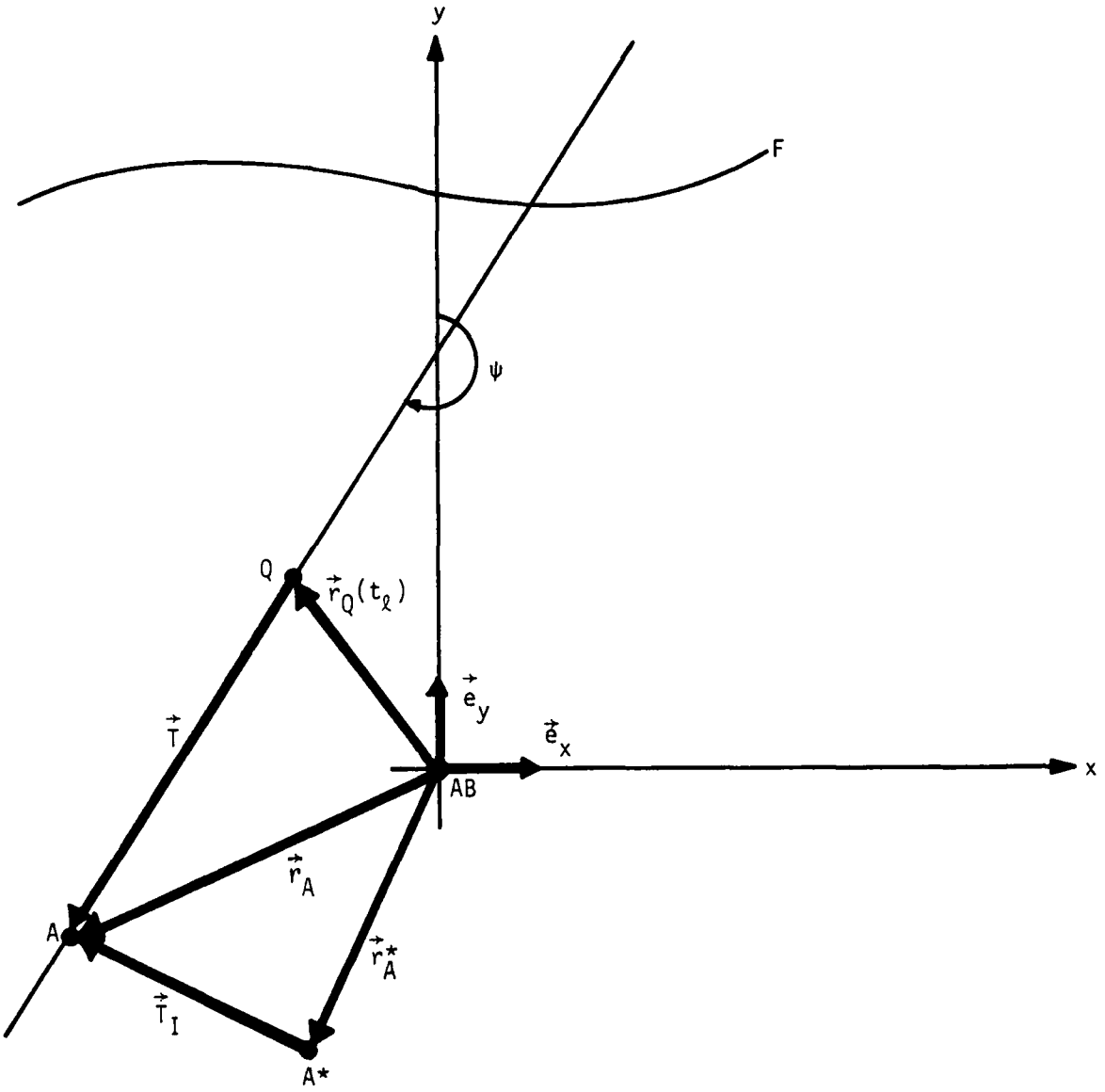

Figure 7. Intercept Geometry - Overhead View

$$\vec{T}_I = (t_a - t_\ell)\,\vec{v}_I \tag{50}$$

$$\vec{T} = (t_A - t_\ell)\,\vec{v} \tag{51}$$

$$\vec{r}_A = \vec{r}_Q(t_\ell) + \vec{T} \tag{52}$$

$$\vec{r}_A = \vec{r}_A^{\,*} + \vec{T}_I \tag{53}$$

Equations (49) through (53) allow us to calculate t_A and $\vec{r}_A$ which are needed in equation (48). First we combine equations (52) and (53) to get

$$\vec{T}_I = \vec{r}_Q(t_\ell) + \vec{T} - \vec{r}_A^{\,*} \tag{54}$$

Inserting equations (50) and (51) gives (56)

$$(t_a - t_\ell)\vec{v}_I = \vec{r}_Q(t_\ell) + (t_A - t_\ell)\,\vec{v} - \vec{r}_A^{\,*} \tag{55}$$

Finally, inserting equation (49) gives

$$[t_A - (t_\ell + \tau_L + \tau_S)]\vec{v}_I = \vec{r}_Q(t_\ell) + (t_A - t_\ell)\,\vec{v} - \vec{r}_A^{\,*}$$

The following auxiliary relations simplify the notation:

$$\vec{W} \equiv \vec{r}_Q(t_\ell) - t_\ell\,\vec{v} - \vec{r}_A^{\,*} \tag{57}$$

$$\Theta \equiv t_\ell + \tau_L + \tau_S \tag{58}$$

Equation (56) now becomes

$$(t_A - \Theta)\,\vec{v}_I = t_A\,\vec{v} + \vec{W} \tag{59}$$

Equation (59) is the basic attack equation and represents the intercept geometry. Our goal is to use it to find the attack time t_A, but we cannot use it directly because only the magnitude and not the direction of $\vec{v}_I$ is known. Thus, we first square equation (59) to get the following quadratic equation:

$$(v_I^2 - v^2)t_A^2 - 2(\Theta v_I^2 + \vec{v}\cdot\vec{W})t_A + (\Theta^2 v_I^2 - W^2) = 0 \qquad (60)$$

There are two solutions:

$$t_{A1,2} = A \pm \sqrt{A^2 - B} \qquad (61a)$$

$$A \equiv \frac{\Theta v_I^2 + \vec{v}\cdot\vec{W}}{v_I^2 - v^2} \quad ; \quad B \equiv \frac{\Theta^2 v_I^2 - W^2}{v_I^2 - v^2} \qquad (61b,c)$$

The corresponding attack vectors follow from equations (51) and (52):

$$\vec{r}_{A1,2} = \vec{r}_Q(t_\ell) + (t_{A1,2} - t_\ell)\,\vec{v} \qquad (62)$$

(If the attack position is "past" the penetrator's target, then the kill must not be counted in the $\langle N_K \rangle$ total.)

An understanding of the nature of the double solution arises through a simple example. Consider a penetrator and an interceptor which are flying on a head-on collision course and are separated by a distance d, as is depicted in figure 8. The interceptor has two choices. The first is to fly directly at the penetrator and meet it, and the corresponding attack time is

$$t_{A1} = \frac{d}{v + v_I} \qquad (63a)$$

The second is to fly directly away from the penetrator and allow the penetrator to catch up; and the corresponding attack time is

$$t_{A2} = \frac{d}{v - v_I} \qquad (63b)$$

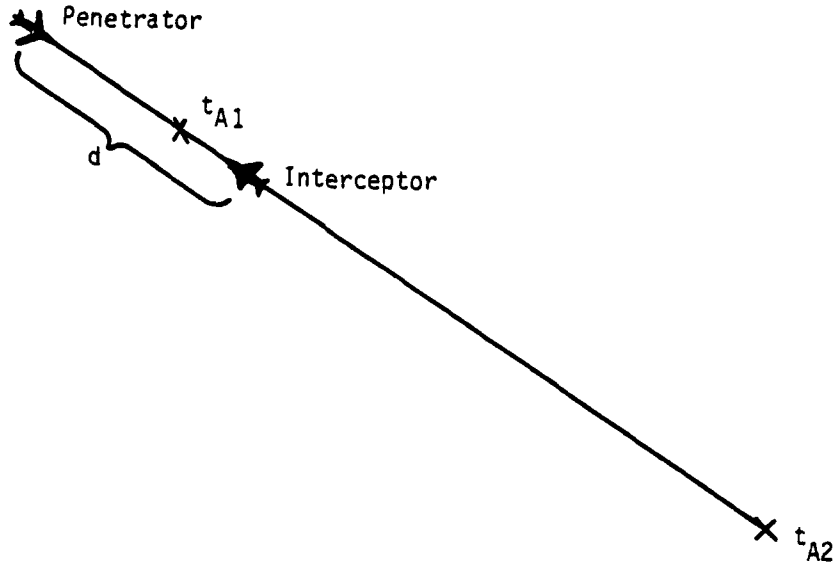

Figure 8. Attack Equation Solutions - An Example

Of course, if the interceptor sustains a velocity $v_I > v$, only t_{A1} has meaning. In addition, if the penetrator is flying directly away from the interceptor, only one attack time exists, namely

$$t_A = \frac{d}{v_I - v} \tag{63c}$$

If in addition $v > v_I$, then no attack times exist.

Precisely the same considerations drive the scheduling problem. The goal is to use equations (61) to first calculate attack times corresponding to the "direct assault" and "catch-up" modes, and then select the earliest meaningful attack time. The attack time is meaningful provided it satisfies the conditions

$$A^2 - B \geq 0 \quad ; \; t_A > t_\ell \tag{64a,b}$$

and a "fuel condition". The latter follows from the observation that, at attack time t_A, the interceptor has traveled the total distance

$$R_I(t_A) \simeq (t_A - \tau_{TO})\, v_I \tag{65}$$

where τ_{TO} is the take-off time. The interceptor can return to the air base if and only if

$$R_I(t_A) + r_A \leq R_I \tag{66}$$

B. VARIED INTERCEPTOR FLIGHT PROFILES

The interceptor must climb to altitude after take-off, be vectored to the first penetrator, and acquire the penetrator with its on-board sensor. If the penetrator flies at a different altitude, and the nature of its weapon system or engagement policy necessitates the interceptor attacking from close range, then homing must occur. The most interesting case involves low-flying penetrators; the interceptor then must dive to home in, attack, and return to cruising altitude after intercept. Figure 9 depicts this flight profile by showing the interceptor climbing from point A* and subsequently diving to point A. The climbing (diving) angle, velocity, and time are γ_C (γ_D), $v_C(v_D)$, and $\tau_C(\tau_D)$, respectively. The penetrator altitude is h (for ease of presentation we assume that all penetrators fly at the same altitude), and the interceptor's cruising altitude is h_I. Figure 9 shows explicitly that vector $\vec{T}_I$ is composed of the climb vector $\vec{r}_C$, cruise vector $\vec{r}_{CR}$, and dive vector $\vec{r}_D$. We now investigate how this flight profile impacts t_A.

The following relations arise from figures 7 and 9:

$$\vec{T}_I = \vec{r}_C + \vec{r}_{CR} + \vec{r}_D \tag{67}$$

$$\vec{r}_{CR} = (t_a - t_\ell - \tau_C - \tau_D)\, \vec{v}_I \tag{68}$$

$$r_C = v_C \tau_C \cos \gamma_C \tag{69}$$

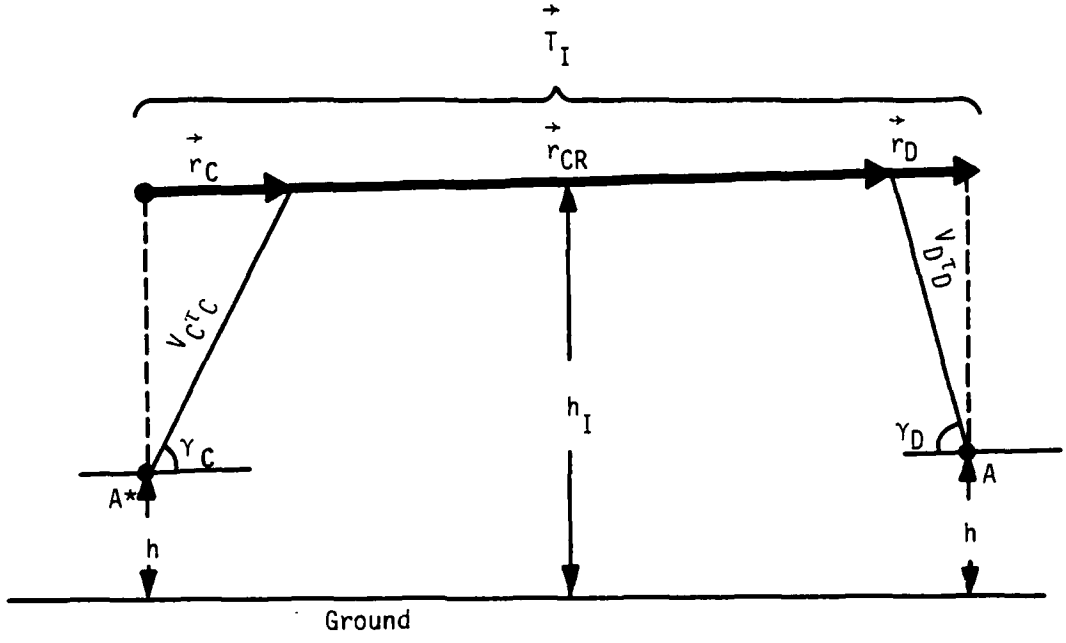

Figure 9. Interceptor Flight Profile Against Low Altitude Penetrators - Side View

$$r_D = v_D \tau_D \cos \gamma_D \tag{70}$$

$$\tau_C = (h_I - h) / v_C \sin \gamma_C \tag{71}$$

$$\tau_D = (h_I - h) / v_D \sin \gamma_D \tag{72}$$

Now, $\vec{r}_C$ and $\vec{r}_D$ both have the same direction as $\vec{v}_I$:

$$\vec{r}_C = r_C \frac{\vec{v}_I}{v_I} \quad ; \quad \vec{r}_D = r_D \frac{\vec{v}_I}{v_I} \tag{73a,b}$$

Combining equations (69) through (73) gives

$$\vec{r}_C = (h_I - h) \cot \gamma_C \frac{\vec{v}_I}{v_I} \tag{74a}$$

$$\vec{r}_D = (h_I - h) \cot \gamma_D \frac{\vec{v}_I}{v_I} \tag{74b}$$

Upon substituting equations (68), (71), (72), and (74) into equation (67), we find

$$\vec{T}_I = [t_a - t_\ell - (\alpha_C + \alpha_D)(h_I - h)]\vec{v}_I \tag{75a}$$

$$\alpha_C \equiv \frac{v_I - v_C \cos \gamma_C}{v_I \, v_C \sin \gamma_C} \quad ; \quad \alpha_D \equiv \frac{v_I - v_D \cos \gamma_D}{v_I \, v_D \sin \gamma_D} \tag{75b,c}$$

By comparing equations (75) and (50), we see the modified attack equation reads

$$[t_A - (\Theta + \tau_{LAG}^{A^* \to A})] \vec{v}_I = t_A \vec{v} + \vec{w} \tag{76a}$$

where[1]

$$\tau_{LAG}^{A^* \to A} \equiv (\alpha_C + \alpha_D)(h_I - h) \tag{76b}$$

The modified attack time solutions are those of equations (61) and with Θ replaced by $\Theta + \tau_{LAG}^{A^* \to A}$.

For the initiation of the attack sequence, beginning with take-off (h=0) and proceeding to the attack of the first penetrator, we set

$$\tau_{LAG}^{0 \to 1} = \alpha_C h_I + \alpha_D (h_I - h) \tag{77}$$

---

1. The authors admit with regret that this symbol suffers from elephantiasis.

Likewise, to finalize the attack sequence, concluding with the last attack followed by landing, we set

$$\tau_{LAG}^{q\to 0} = \alpha_C (h_I - h) + \alpha_D h_I \tag{78}$$

where q denotes the total number of penetrators engageable by the interceptor, that is, the weapon load.

C. DEVECTORING THE ATTACK EQUATIONS

The attack equations must now be written in component form to allow for programming. In addition, we must evaluate terms like $\vec{v} \cdot \vec{W}$ and W^2; this can be done using the penetrator heading ψ. Let us begin by writing $\vec{v}$ and $\vec{W}$ with respect to the basis vectors $\vec{e}_x$ and $\vec{e}_y$ in figure 7:

$$\vec{v} = v \sin\psi \, \vec{e}_x + v \cos\psi \, \vec{e}_y \tag{79}$$

$$\vec{r}_Q(t_\ell) = x_Q(t_\ell)\vec{e}_x + y_Q(t_\ell) \, \vec{e}_y \tag{80}$$

$$\vec{r}_A^{\,*} = x_A^* \, \vec{e}_x + y_A^* \, \vec{e}_y \tag{81}$$

Inserting these into equations (57) gives

$$\vec{W} = W_x \, \vec{e}_x + W_y \, \vec{e}_y \tag{82a}$$

$$W_x = x_Q(t_\ell) - vt_\ell \sin\psi - x_A^* \tag{82b}$$

$$W_y = y_Q(t_\ell) - vt_\ell \cos\psi - y_A^* \tag{82c}$$

It now follows that

$$\vec{v} \cdot \vec{W} = W_x \, v \sin\psi + W_y \, v \cos\psi \tag{83}$$

$$W^2 = W_x^2 + W_y^2 \tag{84}$$

Inserting equations (83) and (84) into equations (61) allows for a direct calculation of the attack time solutions. The component forms of the corresponding attack vectors then follow from equation (62):

$$\vec{r}_{A1,2} = [x_Q(t_\ell) + (t_{A1,2} - t_\ell)\, v \sin\psi]\, \vec{e}_x + \\ + [y_Q(t_\ell) + (t_{A1,2} - t_\ell) v \cos\psi]\, \vec{e}_y \qquad (85)$$

IV. MANEUVERS AND HOMING SIMULATION

Airbreathing strategic penetrators generally will have maneuver capability and will use this capability to evade intercept. This fact makes the deterministic vector analysis approach of the last section too simplistic by itself, yet the probabilistic approach from section II adds the necessary sophistication. That approach allows for homing simulation. Homing, in turn, is contingent on C^3 capability. Given the C^3 capability, one can in principle calculate the average attack times and attack positions by averaging over all possible intercept geometries. However, several difficulties arise which make this direct approach impractical. First is the fact that the averaging process is highly complicated. This is compounded by the nature of the intercept geometry. As we saw through the simple example depicted in figure 8, not all geometries allow for meaningful attack time solutions. Consequently, infinite average attack times are sometimes possible. This suggests to truncate the averaging process, but the question is how? In other words, we need a selection rule. This section presents an indirect, and therefore approximate, scheme which couples C^3 capability, the penetrator-interceptor configuration, and penetrator maneuver capability to (1) the definition of a selection rule for viable attacks, (2) the calculation of the corresponding expected attack times and positions, and (3) the calculation of the corresponding expected P_Ks. The scheme couples the probabilistic approach to the intercept geometry. This section begins with the best case -- continuous vectoring information update, then turns to the worst case -- no update, and finishes with the intermediate case -- periodic update.

A. CONTINUOUS VECTORING UPDATE

Continuous update of vectoring information allows for homing in the purest sense; penetrator maneuvers drive interceptor maneuvers. We have already described penetrator maneuvers in terms of a perturbation approach which centers on a straight line expected path. Consistent with this approach, we now discuss interceptor maneuvers in terms of an expected path. Doing so is the heart of our scheme for incorporating interceptor homing.

The case of continuous update is represented by figure 10. It shows the penetrator starting at point $<P(t_\ell)>$ which is the expected penetrator

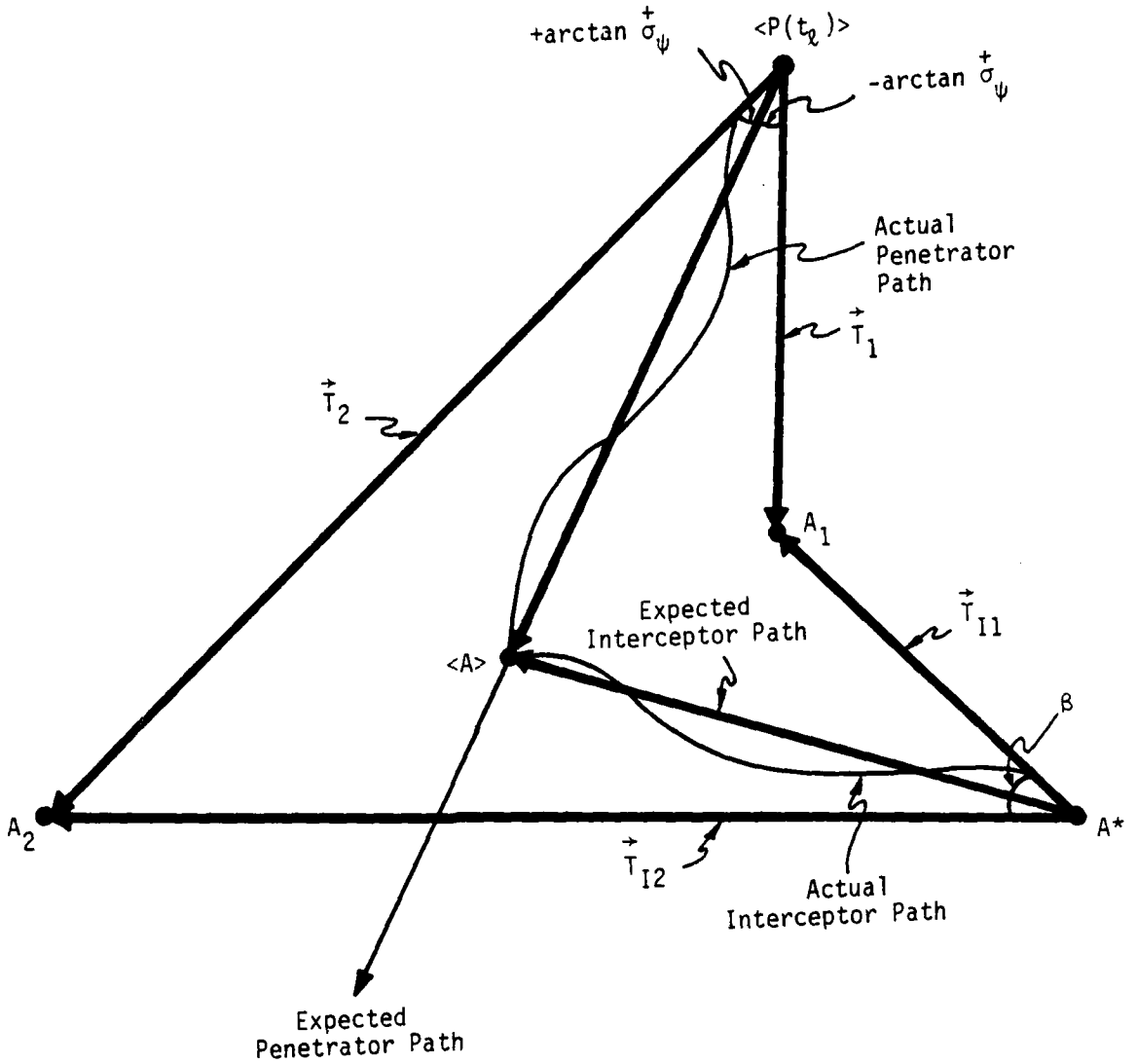

Figure 10. Intercept Geometry - Continuous Update

position at time t_ℓ from the analyst's point of view. The point $<P(t_\ell)>$ for the maneuvering penetrator now replaces the point Q of figure 7 for the non-maneuvering penetrator. In parallel to equations (8) and (9), $<P(t_\ell)>$ is given by

$$<x(t_\ell)> = x_F + v_e \sin<\hat{\psi}> (t_\ell - t_F) \tag{86a}$$

$$<y(t_\ell)> = y_F + v_e \cos<\hat{\psi}> (t_\ell - t_F) \tag{86b}$$

At the same time t_ℓ, the interceptor leaves point A* where it attacked the previous penetrator. The maneuvering of the present penetrator causes the interceptor to maneuver, too, while homing. We characterize interceptor maneuvers in terms of an expected path which we approximate at the outset to be linear. The interceptor then moves along its expected path with speed $v_{Ie} < v_I$ to execute attack at the expected attack point <A>. Our problem now reduces to estimating v_{Ie}. In the perturbation approach, we stated that a given penetrator was equally likely to deviate from its expected path by an angle $+\overset{+}{\psi}$ as by $-\overset{+}{\psi}$. Figure 10 shows two such deviations at point $<P(t_\ell)>$ -- one corresponding to $+\overset{+}{\psi} = +\arctan \overset{+}{\sigma}_\psi$, and the other corresponding to $-\overset{+}{\psi} = -\arctan \overset{+}{\sigma}_\psi$. We structure the estimate of v_{Ie} on these two "root-mean-square" maneuvers.

The attack points A_1 and A_2 correspond to the deviations $-\arctan \overset{+}{\sigma}_\psi$ and $+\arctan \overset{+}{\sigma}_\psi$, respectively. They are calculated by using the basic equations of section III. The attack times corresponding to A_1 and A_2 follow from equations (61) and have the form

$$t_A(A_{1,2}) = t_A \left(\psi = <\overset{+}{\psi}> \mp \arctan\sigma_\psi^+\right) \tag{87}$$

The corresponding attack vectors then follow from equation (62). They have the form

$$\vec{r}_A(A_{1,2}) = <\vec{r}(t_\ell)> + [t_A(A_{1,2}) - t_\ell]\, \vec{v} \tag{88}$$

where $<\vec{r}(t_\ell)>$ is the radius vector to $<P(t_\ell)>$. Finally, the corresponding interceptor transit vectors follow from equation (53):

$$\vec{T}_{I1,2} = \vec{r}_A(A_{1,2}) - \vec{r}_A^* \tag{89}$$

Our selection rule then is to require that the attack points A_1 and A_2 both be physically real, that is, that they correspond to meaningful attack times satisfying the conditions of equations (64) and (66). Should the penetrator-interceptor configuration be such that the selection rule cannot be satisfied, then the attack is aborted.

We now can tie down <A> based on figure 10. The angle β between the two interceptor transit vectors is

$$\beta = \arccos\left[\frac{\vec{T}_{I1} \cdot \vec{T}_{I2}}{T_{I1}\ T_{I2}}\right] \tag{90}$$

We then take for the effective interceptor speed along its expected path

$$v_{Ie} \simeq v_I \cos(\beta/2) \tag{91}$$

Finally, we substitute this speed and the effective penetrator speed into equations (61) and (62) to estimate the expected attack time and corresponding attack position:

$$t_A(<A>) \simeq t_A\ (<\hat{\psi}>,\ v_e,\ v_{Ie}) \tag{92a}$$

$$\vec{r}_A(<A>) \simeq \vec{r}_A\ [t_A[(<A>),\ v_e] \tag{92b}$$

It now remains to outline the corresponding $<P_K>$ calculation. Let us assume that the C^3 network carries a non-zero dead time τ_d. The effects of dead time on the attack calculations depends on the specific nature of the C^3. For example, if the vectoring information is not internally adjusted to compensate for dead time, then the resulting attack point <A> deviates from the expected penetrator position $<P(t_A)>$ at the attack time t_A by a factor of roughly $v\tau_d$.

The major impact of the dead time is on the PDFs of section II. For one, the sensor-induced uncertainties will correspond to a time earlier than the attack time:

$$\hat{\sigma}(t_A) \rightarrow \hat{\sigma}[t_A(<A>) - \tau_d] \tag{93}$$

In addition, we have in the PDFs

$$\rho(t_A) \simeq v_\chi \tau_d \tag{94}$$

This equation plays the role of equation (32c) in the $<P_K>$ calculation. Integration then proceeds according to the prescription of equation (48). The resulting $<P_K>$ generally will be largest given continuous update; this is the best case.

B. NO VECTORING UPDATE

Having no update of vectoring information precludes interceptor homing. In this case, the interceptor attack is based on the last information received, and the interecept geometry of figure 7 represents the calculation of the expected attack position <A>. Let us assume that the last information was received at time $t_o \leq t_\ell$. Then the point $<P(t_\ell)>$ in figure 7 is defined by

$$<x(t_\ell)> = x_F + [(t_o - t_F)v_e + (t_\ell - t_o)<\hat{v}>] \sin<\hat{\psi}> \tag{95a}$$

$$<y(t_\ell)> = y_F + [(t_o - t_F)v_e + (t_\ell - t_o)<\hat{v}>] \cos<\hat{\psi}> \tag{95b}$$

The attack times and attack positions now follow directly from equations (61) and (62).

The $<P_K>$ corresponding to no vectoring update will generally be smallest because the errors in the sensor-predicted penetrator position at time t_A will generally be largest. This is the worst case.

C. PERIODIC VECTORING UPDATE

Let us now suppose vectoring information is periodically received with the period τ_v. Then the average separation of the attack time and the last update is $\tau_v/2$. An approximate solution of the corresponding homing

problem involves a combination of the techniques explained in subsections A and B and is represented by figure 11. We first calculate the attack time t_A and attack position A' corresponding to continuous update from equations (92). We next subtract $\tau_v/2$ from t'_A to find the "intermediate time"

$$t_{IN} \equiv t'_A - \tau_v/2 \tag{96}$$

At times between t_{IN} and t'_A, sensor information is unavailable. We next find the corresponding intermediate attack point $<P_I(t_{IN})>$ which is the expected interceptor position at the time t_{IN} from the analyst's point of view. This point, shown in figure 11, is given by

$$<\vec{r}_{IN}> = (t_{IN} - t_\ell)\, v_{Ie}\, \frac{<\vec{r}'_A>}{<r'_A>} \tag{97}$$

Here, $<\vec{r}_{IN}>$ is the radius vector to $<P_I(t_{IN})>$, and $<\vec{r}'_A>$ is the radius vector to <A'>. While the interceptor flies to $<P_I(t_{IN})>$, the penetrator flies to the intermediate position $<P(t_{IN})>$ represented by

$$<x(t_{IN})> = <x(t_\ell)> + v_e \sin<\hat{\psi}> (t_{IN} - t_\ell) \tag{98a}$$

$$<y(t_{IN})> = <y(t_\ell)> + v_e \cos<\hat{\psi}> (t_{IN} - t_\ell) \tag{98b}$$

The points $<P_I(t_{IN})>$ and $<P(t_{IN})>$ now serve as the initial interceptor point and initial penetrator point. Because t_{IN} marks the termination of vectoring information, we now revert to the no update formalism. The attack time t_A and attack position <A> estimates then follow from equations (61) and (62).

If τ_v is small, then it follows that the major impact is on the PDFs in parallel to equations (93) and (94), except now τ_d is replaced with $\tau_d + \tau_v/2$. The resultant $<P_K>$ is generally smaller than that of continuous update, but is generally larger than that of no update. Periodic update is the intermediate case.

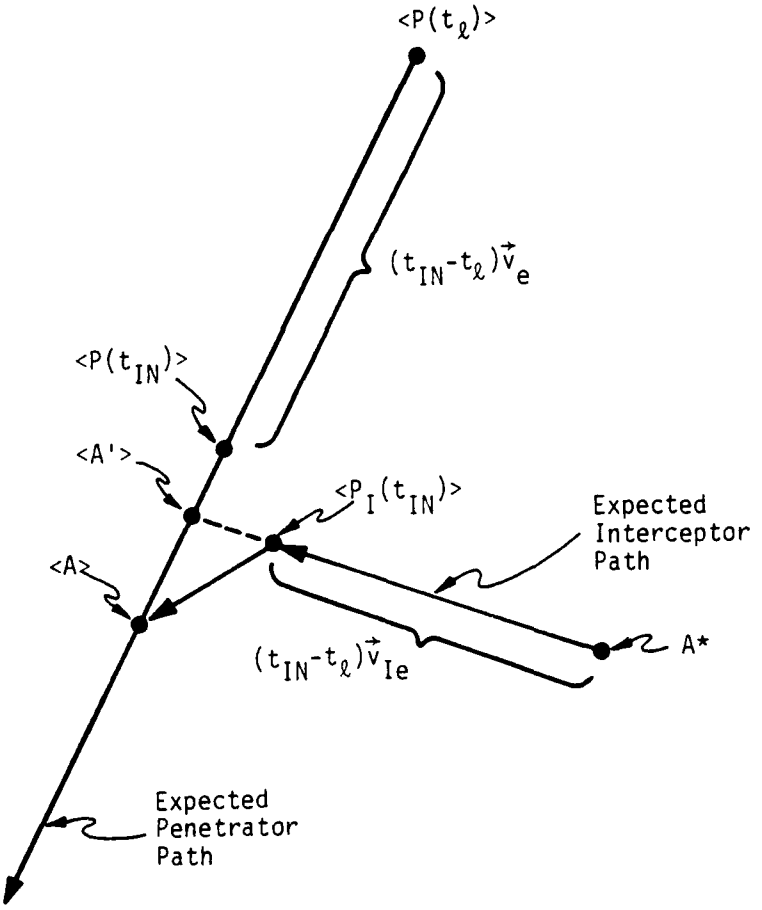

Figure 11. Intercept Geometry - Periodic Update

V. GUIDED AAM STANDOFF ATTACK -- AN EXAMPLE

Our air defense formalism can be applied to virtually any air defense system predicated on airborne platforms. To illustrate one such application, let us consider standoff attack against the strategic penetrators. Specifically, let us consider a hypothetical futuristic weapon system based on long-range air-to-air missiles. The weapon platform is given continuous vectoring information update. This section outlines the application of our formalism to model this air defense system.

The missile flight makes the representation of standoff missile attack slightly more complicated than that of close-range attack. In figure 12, which shows the standoff attack intercept geometry, the attack point A is detached from the penetrator's path. The missile flies from A along vector $\vec{m}$ to kill the penetrator at the kill time t_K and the kill position K which is represented by the vector $\vec{r}_K$. The magnitude of $\vec{m}$ is taken as a parameter which depends on the operational missile firing range R_M (generally less than the missile's total range capability):

$$m = R_M \tag{99}$$

Likewise, in the absence of penetrator maneuvers, the missile flight time is a parameter depending on R_M and the missile speed v_M:

$$\tau_M = R_M/v_M \tag{100}$$

Apart from these missile-induced modifications, the intercept geometry is the same as that for close-range attack (see figure 7).

Given that the penetrator maneuvers, the present problem decomposes into two separate homing problems. The first is the homing of the interceptor toward the expected attack position <A>. The second is the homing of the missile from <A> toward the expected kill position <K>. We begin with the calculation of <A> in parallel to sections III and IV.

In parallel to equations (49) - (53), the intercept geometry gives rise to the following relations:

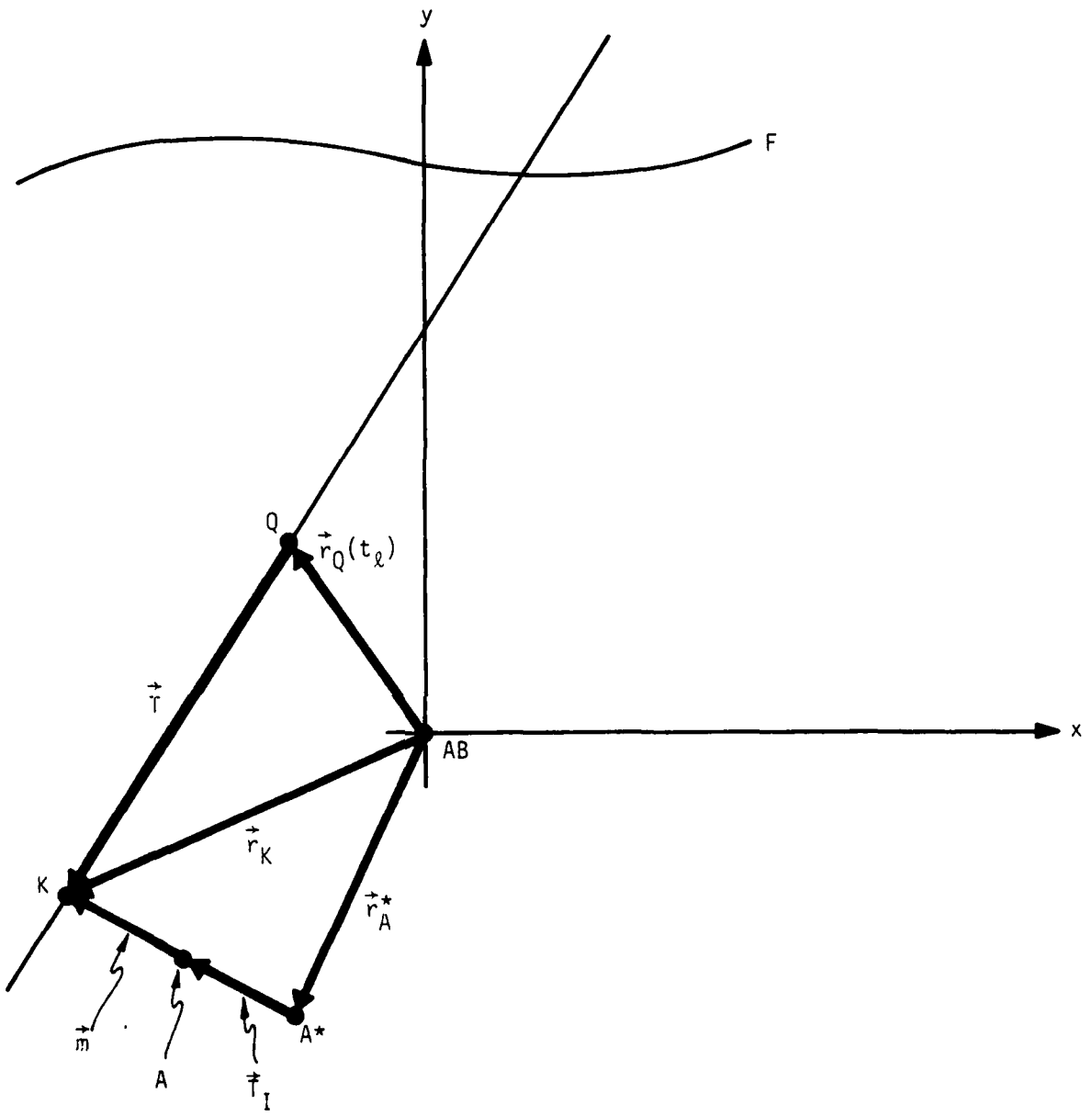

Figure 12. Guided AAM Standoff Attack Intercept Geometry

$$t_K = t_A + \tau_M + \tau_L + \tau_S \tag{101}$$

$$t_A = t_K - \tau_M \tag{102}$$

$$\vec{T}_I = (t_a - t_\ell)\ \vec{v}_I \tag{103}$$

$$\vec{T} = (t_K - t_\ell)\ \vec{v} \tag{104}$$

$$\vec{r}_K = \vec{r}_Q(t_\ell) + \vec{T} \tag{105}$$

$$\vec{r}_K = \vec{r}_A^{\,*} + \vec{T}_I + \vec{m} \tag{106}$$

To calculate the attack time t_A, we combine these equations and find

$$(t_A - \Theta)\ \vec{v}_I + \vec{m} = t_A\ \vec{v} + \vec{W}_M \tag{107a}$$

$$\vec{W}_M \equiv \vec{r}_Q(t_\ell) - (t_\ell - \tau_M)\ \vec{v} - \vec{r}_A^{\,*} \tag{107b}$$

$$\Theta \equiv t_\ell + \tau_L + \tau_S \tag{107c}$$

Squaring equation (107a) gives

$$(v_I^2 - v^2)t_A^2 - 2(\Theta v_I^2 + \vec{v} \cdot \vec{W}_M - v_I R_M)t_A + (r_M^2 + \Theta^2 v_I^2 + 2\Theta v_I R_M - W_M^2) = 0 \tag{108}$$

The solutions are

$$t_{A1,2} = A_M \pm \sqrt{A_M^2 - B_M} \tag{109a}$$

$$A_M \equiv \frac{\Theta v_I^2 + \vec{v} \cdot \vec{W}_M - v_I R_M}{v_I^2 - v^2} \tag{109b}$$

$$B_M \equiv \frac{R_M^2 + \Theta^2\ v_I^2 + 2\Theta\ v_I\ R_M - W_M^2}{v_I^2 - v^2} \tag{109c}$$

These solutions do not reflect penetrator maneuvers. Rather, they are tools to be used in the homing calculations set forth in section IV. The expected attack time $t_A(<A>)$ and attack position $\vec{r}_A(<A>)$ follow from the recipe represented by equations (92). The expected attack position $<A>$ now forms the basis for calculating the expected kill position $<K>$. The problem geometry corresponding to missile flight is identical to the close range intercept geometry of figure 7. Thus, we merely replace A by $<A>$, v_I by v_M, and t_ℓ by $t_A(<A>)$, and then use the formalism of sections III and IV directly to calculate $<K>$ and $t_K(<K>)$. The expected attack times and positions impact $<P_K>$ through equation (48) and interceptor scheduling, while the expected kill times and positions impact $<N_K>$.

VI. SUMMARY

The methodology presented in this paper is designed to model a complicated strategic defense configuration. It relies on a wide variety of inputs to characterize geography, force structure, and system parameters. For modelling the close-range (one-on-one) intercept problem the required inputs are:

Geography[1] - fence configuration, coordinates of: air bases, home/staging bases, US targets, recovery bases, surveillance sensors.

Force Structure - penetrator scheduling against US targets, number of penetrators per home/staging base, number of interceptors per interceptor base.

System Parameters -

penetrator: R_p, v, h, $\overset{+}{\sigma}_v$, $\overset{+}{\sigma}_\psi$

interceptor: R_I, v_I, h_I, γ_C, γ_D, v_C, v_D, q, τ_S, P_K envelope

surveillance sensor: σ_R, σ_{EL}, σ_{AZ}, σ_{vR}, σ_{vEL}, σ_{vAZ}, P_D envelope

C^3: τ_d, τ_v

Some of the inputs may require separate models; examples are P_K and τ_S.

The calculations of expected attack times and positions and expected kill probabilities now proceed along the following sequence[2]:

Step 1 - Calculate v_e from equation (11).

---

1. Depending on user needs, all geography inputs can be either abstract or derived directly from force structure and weapon laydown considerations.

2. For concreteness we have set forth the sequence which corresponds to the continuous vectoring update case.

Step 2 - For each interceptor - penetrator configuration, calculate the earliest $t_A(A)$ from equations (87) and (61). Abort attacks not satisfying the conditions set forth in equations (64) and (66).

Step 3 - For interceptor - penetrator configurations surviving Step 2, calculate $\vec{r}_A(A)$ from equation (88).

Step 4 - Calculate $\vec{T}_{I1,2}$ from equation (89).

Step 5 - Calculate v_{Ie} from equation (91).

Step 6 - Calculate the earliest $t_A(\langle A \rangle)$ from equations (92) and (61). Abort attacks not satisfying the conditions set forth in equations (64) and (66).

Step 7 - Calculate $\vec{r}_A(\langle A \rangle)$ from equation (62).

Step 8 - Calculate $\hat{\sigma}_x$, $\hat{\sigma}_y$, $\hat{\sigma}_z$, $\hat{\sigma}_v$, and $\hat{\sigma}_\psi$ from equations (19), (20), and (21).

Step 9 - Calculate $\langle P_K(x_A, y_A, z_A) \rangle$ from equation (48).

In summary, the methodology combines surveillance sensor, interceptor, and C^3 capabilities into an overall air defense simulation model to serve as a basis for assessing performance of weapon systems relying on airborne platforms. Because it can accept any geographic configuration, be it abstract or real, it allows for modelling a variety of scenarios. Furthermore, it incorporates maneuver capability of airbreathing penetrators into a straightforward probabilistic approach to generate closed form solutions which are amenable to direct scheduling. In this way, the methodology facilitates efficient, time-saving programming. Finally, and perhaps most importantly, it provides the tools for a direct sensitivity analysis of overall weapon system performance to tracking errors and other determinants.

APPENDIX A

TRANSFORMATION OF STANDARD DEVIATIONS

This appendix details the calculations which transform sensor-induced down-range and cross-range standard deviations into the cartesian standard deviations listed in equations (19), (20), and (21).

A. CALCULATION OF $\hat{\sigma}_x(t_o)$, $\hat{\sigma}_y(t_o)$, $\hat{\sigma}_z(t_o)$

Figure A1 shows the cartesian coordinate system (x_S, y_S, z_S) centered on the sensor S. The penetrator is at point $P(t_o)$ with the coordinates $[x_{SP}(t_o)$, $y_{SP}(t_o)$, $z_{SP}(t_o),]$. The following relations derive from the figure:

$$x_{SP}(t_o) = r_{SP}(t_o) \sin[\theta(t_o)] \cos[\phi(t_o)] \tag{A1a}$$

$$y_{SP}(t_o) = r_{SP}(t_o) \sin[\theta(t_o)] \sin[\phi(t_o)] \tag{A1b}$$

$$z_{SP}(t_o) = r_{SP}(t_o) \cos[\theta(t_o)] \tag{A1c}$$

One can show that the standard deviation associated with a quantity m which is itself a function of many (n) variables can be calculated approximately via a summation process as follows[1]:

$$\hat{\sigma}_m = \sqrt{\sum_{i=1}^{n} \left(\frac{\partial \hat{m}}{\partial x_i}\right)^2 \hat{\sigma}_{xi}^2} \tag{A2}$$

where the coefficients of the standard deviations $\hat{\sigma}_{xi}$ are evaluated by substituting measured values (hence, the presence of the hat-symbol). Direct application of equation (A2) gives

1. Baird, pp. 61-64.

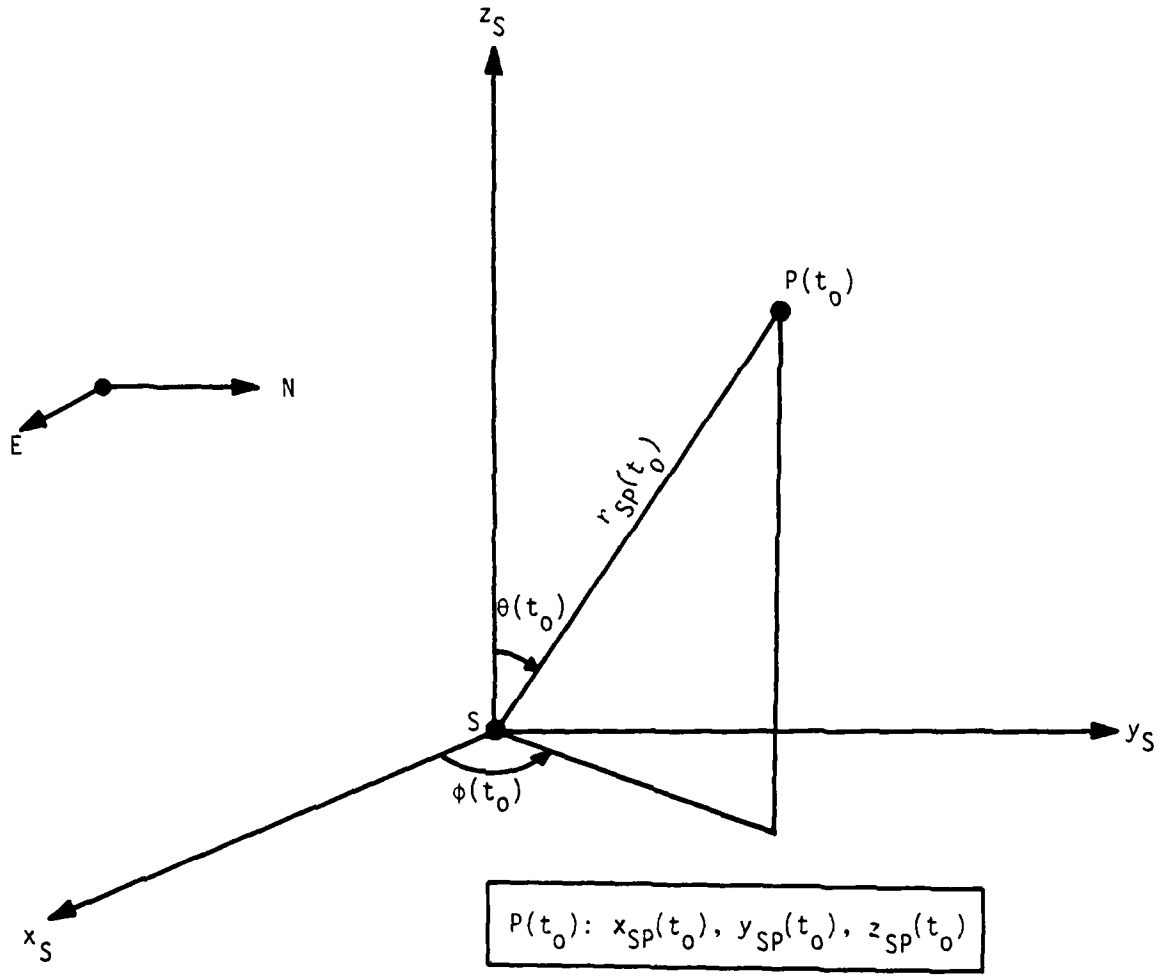

Figure A1. Sensor-Based Cartesian Coordinate System

$$\hat{\sigma}_{xS} = \sqrt{\left(\frac{\partial \hat{x}_S}{\partial r_{SP}}\right)^2 \sigma_R^2 + \left(\frac{\partial \hat{x}_S}{\partial \theta}\right)^2 \sigma_{EL}^2 + \left(\frac{\partial \hat{x}_S}{\partial \phi}\right)^2 \sigma_{AZ}^2} \qquad \text{(A3)}$$

and likewise for $\hat{\sigma}_{yS}$ and $\hat{\sigma}_{zS}$. We drop the hat-symbol from $\hat{\sigma}_R$, $\hat{\sigma}_{EL}$, $\hat{\sigma}_{AZ}$ because these obviously refer to the sensor.

It remains to convert to "air base" coordinates. Figure A2 implies that

$$\vec{r}_{SP}(t_o) = \vec{r}_{BP}(t_o) - \vec{r}_{BS}(t_o) \qquad \text{(A4)}$$

where the subscripts "SP", "BP", and "BS" stand for "sensor-to-penetrator", "base-to-penetrator", and "base-to-sensor". Note that $\vec{r}_{BS}$ really is time-dependent if the sensor is mobile. If we ignore errors in $\vec{r}_{BS}$, then it follows for equation (A4) and figure A2 that

$$\hat{\sigma}_x(t_o) = \hat{\sigma}_{xS}(t_o);\ \hat{\sigma}_y(t_o) = \hat{\sigma}_{yS}(t_o);\ \hat{\sigma}_z(t_o) = \hat{\sigma}_{zS}(t_o) \qquad \text{(A5a,b,c)}$$

Thus, a direct substitution of equations (A1) into equation (A3) results in equations (19), and equations (21) follow from equations (A1) and (A4).

B. CALCULATION OF $\hat{\sigma}_v(t_o)$

We are considering penetrators constrained to a horizontal plane; the cartesian velocity components are

$$v_x = v \sin\psi;\ v_y = v \cos\psi \qquad \text{(A6a, b)}$$

The corresponding velocity components $v_r(t_o)$, $v_\theta(t_o)$, $v_\phi(t_o)$ in a spherical coordinate system centered on the sensor are related to v_x and v_y through an orthonormal transformation matrix $M(t_o)$:

$$\begin{bmatrix} v_x \\ v_y \\ 0 \end{bmatrix} = M \begin{bmatrix} v_r \\ v_\theta \\ v_\phi \end{bmatrix} \quad ; \quad \begin{bmatrix} v_r \\ v_\theta \\ v_\phi \end{bmatrix} = M^T \begin{bmatrix} v_x \\ v_y \\ 0 \end{bmatrix} \qquad \text{(A7a,b)}$$

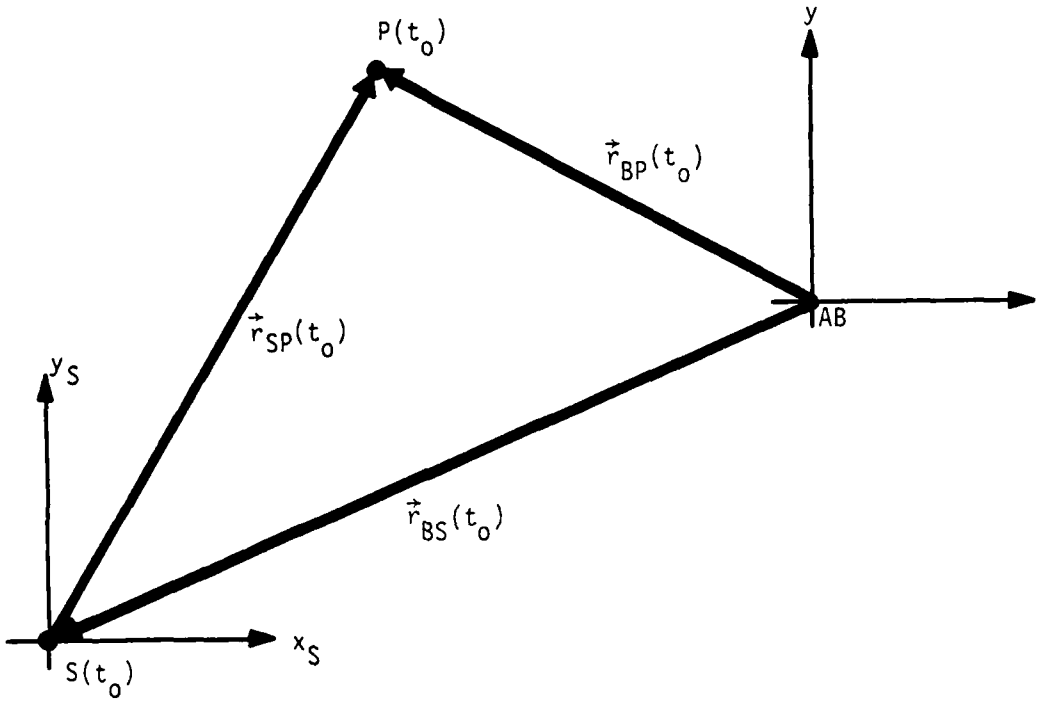

Figure A2. Sensor Coordinates Vs Air Base Coordinates

$$M(t_o) = \begin{bmatrix} \sin[\theta(t_o)]\cos[\phi(t_o)] & \cos[\theta(t_o)]\cos[\phi(t_o)] & -\sin[\phi(t_o)] \\ \sin[\theta(t_o)]\sin[\phi(t_o)] & \cos[\theta(t_o)]\sin[\phi(t_o)] & \cos[\phi(t_o)] \\ \cos[\theta(t_o)] & -\sin[\theta(t_o)\,] & 0 \end{bmatrix} \quad \text{(A7c)}$$

Now, the penetrator speed is simply

$$v = \sqrt{v_r^2 + v_\theta^2 + v_\phi^2} \quad \text{(A8)}$$

An application of equation (A2) gives

$$\hat{\sigma}_v(t_o) = \sqrt{\left(\frac{\hat{v}_r(t_o)}{\hat{v}}\right)^2 \sigma_{vR}^2 + \left(\frac{\hat{v}_\theta(t_o)}{\hat{v}}\right)^2 \sigma_{vEL}^2 + \left(\frac{\hat{v}_\phi(t_o)}{\hat{v}}\right)^2 \sigma_{vAZ}^2} \quad \text{(A9)}$$

Substituting equations (A7b) and (A6) into equation (A9) gives equation (20a).

C. CALCULATION OF $\hat{\sigma}_\psi(t_o)$

Equations (A6) imply that

$$\tan\psi = \frac{v_x}{v_y} \quad \text{(A10)}$$

from which

$$\frac{\partial \tan\psi}{\partial v_r} = \frac{\partial \tan\psi}{\partial v_x}\,\frac{\partial v_x}{\partial v_r} + \frac{\partial \tan\psi}{\partial v_y}\,\frac{\partial v_y}{\partial v_r} \quad \text{(A11)}$$

Using equation (A7a) we find

$$\frac{\partial \hat{\tan\psi}}{\partial v_r} = \frac{\sin[\hat{\theta}(t_o)]\,\cos[\hat{\psi} + \hat{\phi}(t_o)]}{\hat{v}\,\cos^2\hat{\psi}} \quad \text{(A12a)}$$

In the same way we also find

$$\frac{\partial \hat{\tan\psi}}{\partial v_\theta} = \frac{\cos[\hat{\theta}(t_o)]\ \cos[\hat{\psi} + \hat{\phi}(t_o)]}{\hat{v}\cos^2\hat{\psi}} \qquad \text{(A12b)}$$

$$\frac{\partial \hat{\tan\psi}}{\partial v_\phi} = \frac{-\sin[\hat{\psi} + \hat{\phi}(t_o)]}{\hat{v}\cos^2\hat{\psi}} \qquad \text{(A12c)}$$

Direct application of equation (A2) followed by substitution of equations (A12) yields equation (20b).

APPENDIX B

CONVOLUTION INTEGRALS AND MOMENT EXPANSIONS

This appendix explains the approximation procedure which converts equations (36) into equations (37). To this end, we observe that equations (37) describe an averaging process over $\hat{\mu}$ and $\overset{+}{\mu}$. Hence we may write

$$X[x(t)] = \langle G_x(\hat{\mu}, \overset{+}{\mu}) \rangle \tag{B1a}$$

$$Y[y(t)] = \langle G_y(\hat{\mu}, \overset{+}{\mu}) \rangle \tag{B1b}$$

We first develop the functions to be averaged, G_x and G_y, as Taylor series in $\hat{\mu}$ and $\overset{+}{\mu}$ in the neighborhood of $\langle\hat{\mu}\rangle$ and $\langle\overset{+}{\mu}\rangle$. If we then carry out the averaging process and if we observe the statistical independence of $\hat{\mu}$ and $\overset{+}{\mu}$, we obtain

$$X[x(t)] = G_x(\langle\hat{\mu}\rangle, \langle\overset{+}{\mu}\rangle) + \langle\Delta\hat{\mu}\rangle \frac{\partial G_x}{\partial \hat{\mu}}(\langle\hat{\mu}\rangle, \langle\overset{+}{\mu}\rangle) +$$

$$+ \langle\Delta \overset{+}{\mu}\rangle \frac{\partial G_x}{\partial \overset{+}{\mu}} (\langle\hat{\mu}\rangle, \langle\overset{+}{\mu}\rangle) + \langle\Delta\hat{\mu}\rangle\langle\Delta\overset{+}{\mu}\rangle \frac{\partial^2 G_x}{\partial\hat{\mu}\,\partial\overset{+}{\mu}} (\langle\hat{\mu}\rangle, \langle\overset{+}{\mu}\rangle) +$$

$$+ \frac{1}{2}\langle(\Delta\hat{\mu})^2\rangle \frac{\partial^2 G_x}{\partial\hat{\mu}^2}(\langle\hat{\mu}\rangle, \langle\overset{+}{\mu}\rangle) +$$

$$+ \frac{1}{2}\langle(\Delta\overset{+}{\mu})^2\rangle \frac{\partial^2 G_x}{\partial\overset{+}{\mu}^2} (\langle\hat{\mu}\rangle, \langle\overset{+}{\mu}\rangle) + \ldots \tag{B2a}$$

$$\Delta\hat{\mu} \equiv \hat{\mu} - \langle\hat{\mu}\rangle \qquad \Delta\overset{+}{\mu} \equiv \overset{+}{\mu} - \langle\overset{+}{\mu}\rangle \tag{B2b,c}$$

Here, we note, for example, that $\langle(\hat{\mu}-\langle\hat{\mu}\rangle)\rangle = 0$, that $\langle\overset{+}{\mu}\rangle = 0$, and that $\langle(\hat{\mu}-\langle\hat{\mu}\rangle)^2\rangle = \hat{\sigma}^2_{\psi}$. If we neglect terms higher than second order, we obtain

$$X[x(t)] = G_x(\langle\hat{\mu}\rangle, 0) + \frac{1}{2}\hat{\sigma}_\psi^2 \frac{\partial^2 G_x}{\partial\hat{\mu}^2}(\langle\hat{\mu}\rangle, 0) + \frac{1}{2}\sigma_\psi^{+2}\frac{\partial^2 G_x}{\partial\mu^{+2}}(\langle\hat{\mu}\rangle, 0) \quad \text{(B3a)}$$

In exactly the same way, we also find

$$Y[y(t)] = G_y(\langle\hat{\mu}\rangle, 0) + \frac{1}{2}\hat{\sigma}_\psi^2 \frac{\partial^2 G_y}{\partial\hat{\mu}^2}(\langle\hat{\mu}\rangle, 0) + \frac{1}{2}\sigma_\psi^{+2}\frac{\partial^2 G_y}{\partial\mu^{+2}}(\langle\hat{\mu}\rangle, 0) \quad \text{(B3b)}$$

It remains to calculate the derivatives. To this end, we write equation (36c) in the shorthand form

$$\sqrt{2\pi}\, G_x = a\, e^{-b} \quad \text{(B4a)}$$

with

$$a \equiv \frac{i}{\sigma_S(t)} \quad \text{(B4b)}$$

$$b \equiv \frac{\Delta x^2(t)}{2\sigma_S^2(t)} \quad \text{(B4c)}$$

$$\Delta x(t) \equiv x(t) - \langle\hat{x}(t_0)\rangle - S\rho(t) \quad \text{(B4d)}$$

We denote derivatives with respect to both $\hat{\mu}$ and $\overset{+}{\mu}$ by primes. Differentiating equation (B4a) then yields

$$\sqrt{2\pi}\, G_x'' = (a'' - 2a'b' - ab'' + a\, b'^2)\, e^{-b} \quad \text{(B5)}$$

From equations (B4b) and (B4c) we get

$$a' = -\frac{\sigma_S'}{\sigma^2} \quad \text{(B6a)}$$

$$a'' = \frac{2\sigma'^2 - \sigma\sigma''}{\sigma^3} \quad \text{(B6b)}$$

$$b' = \frac{\sigma \Delta x \Delta x' - \sigma' \Delta x^2}{\sigma^3} \tag{B6c}$$

$$b'' = \frac{-4\sigma\sigma' \Delta x \Delta x' + \sigma^2 \Delta x'^2 + \sigma^2 \Delta x \Delta x'' - \sigma\sigma'' \Delta x^2 + 3\sigma'^2 \Delta x^2}{\sigma^4} \tag{B6b}$$

Equation (B4d) yields

$$\Delta x' = -S' \rho \tag{B7a}$$

$$\Delta x'' = -S'' \rho \tag{B7b}$$

Finally, from equation (33c), we obtain

$$\sigma_S' = \frac{\sigma_v^2 (t-t_0)^2 S S'}{\sigma_S} \tag{B8a}$$

$$\sigma_S'' = \frac{\sigma_v^2 (t-t_0)^2 [\sigma_S^2 SS'' + \sigma_S^2 S'^2 - \sigma_v^2 (t-t_0)^2 S^2 S'^2]}{\sigma_S^3} \tag{B8b}$$

If now equations (B6), (B7), and (B8) are substituted into equation (B5), it follows after some calculation that

$$G_x'' = \sum_{i=0}^{4} X_i (\Delta x)^i \quad \exp\left[-\frac{(\Delta x)^2}{2\sigma_S^2}\right] \tag{B9a}$$

$$X_4 = \frac{\sigma_v^4 (t-t_0)^4 (S S')^2}{\sigma_S^9 \sqrt{2\pi}} \tag{B9b}$$

$$X_3 = \frac{2\sigma_v^2 (t-t_0)^4 S S'^2 \rho}{\sigma_S^7 \sqrt{2\pi}} \tag{B9c}$$

$$X_2 = \frac{(\rho\sigma_S S')^2 + \sigma_v^2 (t-t_o)^2 \sigma_S^2 (S'^2 + SS'')}{\sigma_S^7 \sqrt{2\pi}} - 6\sigma_S^2 X_4 \qquad \text{(B9d)}$$

$$X_1 = \frac{\rho\sigma_S^2 S'' - 6\rho\sigma_v^2 (t-t_o)^2 \; S S'^2}{\sigma_S^5 \sqrt{2\pi}} \qquad \text{(B9e)}$$

$$X_o = -\sigma_S^2 (3\sigma_S^2 X_4 + X_2) \qquad \text{(B9f)}$$

For the evaluation of the functions X_i, it is necessary to calculate the derivatives of S. From equations (35a) and (35b), we obtain

$$S(\langle\hat{\mu}\rangle, 0) = \sin \langle\hat{\psi}\rangle \qquad \text{(B10a)}$$

$$\frac{\partial S}{\partial \hat{\mu}} (\langle\hat{\mu}\rangle, 0) = \cos^3\langle\hat{\psi}\rangle \; ; \; \frac{\partial S}{\partial \overset{+}{\mu}} (\langle\hat{\mu}\rangle, 0) = \cos \langle\hat{\psi}\rangle \qquad \text{(B10b,c)}$$

$$\frac{\partial^2 S}{\partial \hat{\mu}^2} (\langle\hat{\mu}\rangle, 0) = -3 \sin\langle\hat{\psi}\rangle \cos^4\langle\hat{\psi}\rangle \qquad \text{(B10d)}$$

$$\frac{\partial^2 S}{\partial \overset{+}{\mu}^2} (\langle\hat{\mu}\rangle, 0) = -\sin\langle\hat{\psi}\rangle \qquad \text{(B10e)}$$

Now, returning to equations (B9), we note that it will be necessary to distinguish between differentiations with respect to $\hat{\mu}$ and $\overset{+}{\mu}$. We achieve this by means of the hat and the cross symbols. We have, for example,

$$\hat{G}_x'' = \frac{\partial^2 G_x}{\partial \hat{\mu}^2} = \sum_{i=o}^{4} \hat{X}_i (\Delta x)^i \exp\left(-\frac{\Delta x^2}{2\sigma_s^2}\right) \qquad \text{(B11)}$$

Here the functions $\hat{X}_i$ are obtained by substitution of equations (B10a), (B10b), and (B10d) into equations (B9). In a similar way, we obtain the functions $\overset{+}{X}_i$. The results are represented by equations (37g) through (37p).

An identical set of calculations yields the approximation of $Y[y(t)]$. The functions corresponding to the $\hat{X}_i$ and $\overset{+}{X}_i$ are now $\hat{Y}_i$ and $\overset{+}{Y}_i$. They are represented by equations (37q) through (37z).

If now we combine equations (B3a) and (B5), we obtain

$$X[x(t)] = G_X\,(\langle\hat{\mu}\rangle,\, 0) +$$

$$+ \frac{1}{2} \exp\left(-\frac{\Delta X^2}{2\sigma_S^2}\right) \sum_i (\hat{\sigma}_\psi^2\, \hat{X}_i + \overset{+2}{\sigma}_\psi\, \overset{+}{X}_i)\, (\Delta x)^i \qquad \text{(B12)}$$

Here we introduce

$$X_i = \frac{1}{2}\, \sigma_S\, \sqrt{2\pi}\, (\hat{\sigma}_\psi^2\, \hat{X}_i + \overset{+2}{\sigma}_\psi\, \overset{+}{X}_i) \qquad \text{(B13)}$$

Equation (B3a) may then be written in the form

$$X[x(t)] = G_X(\langle\hat{\mu}\rangle,\, 0) \left[1 + \sum_{i=1}^{4} X_i\, (\Delta x)^i\right] \qquad \text{(B14)}$$

It remains to show that equations (37) are normalized. To this end, we introduce the normalization constants

$$N_X = \int_{-\infty}^{+\infty} X[x(t)]\, dx\,(t) \qquad \text{(B15a)}$$

$$N_y = \int_{-\infty}^{+\infty} Y[y(t)]\, dy\,(t) \qquad \text{(B15b)}$$

We then have

$$N_x = 1 + \frac{1}{2}\hat{\sigma}_\psi^2 \int_{-\infty}^{+\infty} \hat{G}_x'' (\langle\hat{\mu}\rangle, 0)\, dx + \frac{1}{2} \overset{+}{\sigma}{}_\psi^2 \int_{-\infty}^{+\infty} \overset{+}{G}{}_x'' (\langle\overset{+}{\mu}\rangle, 0)\, dx \qquad \text{(B16)}$$

and a corresponding equation for N_y. If we next contemplate substitution of equations (B9) into equation (B16), we get five types of integrals in dx or, what amounts to the same, in $d(\Delta x)$. These are

$$\int_{-\infty}^{+\infty} (\Delta x)^0 \exp\left(-\frac{\Delta x^2}{2\sigma_S^2}\right) d(\Delta x) = \sigma_S \sqrt{2\pi} \qquad \text{(B17a)}$$

$$\int_{-\infty}^{+\infty} (\Delta x)^1 \exp\left(-\frac{\Delta x^2}{2\sigma_S^2}\right) d(\Delta x) = 0 \qquad \text{(B17b)}$$

$$\int_{-\infty}^{+\infty} (\Delta x)^2 \exp\left(-\frac{\Delta x^2}{2\sigma_S^2}\right) d(\Delta x) = \sigma_S^3 \sqrt{2\pi} \qquad \text{(B17c)}$$

$$\int_{-\infty}^{+\infty} (\Delta x)^3 \exp\left(-\frac{\Delta x^2}{2\sigma_S^2}\right) d(\Delta x) = 0 \qquad \text{(B17d)}$$

$$\int_{-\infty}^{+\infty} (\Delta x)^4 \exp\left(-\frac{\Delta x^2}{2\sigma_S^2}\right) d(\Delta x) = 3\,\sigma_S^5 \sqrt{2\pi} \qquad \text{(B17e)}$$

Hence it follows that

$$\int_{-\infty}^{+\infty} \hat{G}_x'' (\langle\hat{\mu}\rangle, 0)\, dx = \sqrt{2\pi}(3\sigma_S^5 \hat{X}_4 + \sigma_S^3 \hat{X}_2 + \sigma_S \hat{X}_o) \qquad \text{(B18)}$$

If equations (37g) through (37k) are observed here, then it follows that this integral vanishes. The same results arise upon integrating over $G_x^{+''}$. Hence we have

$$N_x = 1 \tag{B19a}$$

The same operations on G_y'' give

$$N_y = 1 \tag{B19b}$$

APPENDIX C

THE APVAST COMPUTER PROGRAM

A. CAPABILITIES. The APVAST program is designed to calculate expected number of penetrators killed. It begins by estimating penetrator maneuver tendency based on fuel constraints. Then, for an individual attack, it incorporates the penetrator maneuver tendency into the calculation of the earliest expected attack time and the corresponding attack position of the interceptor. Once this is done, the program turns to finding the associated expected probability of kill. The calculations incorporate the capabilities of both the interceptor and the interceptor weapon. Independent of the nature of the C^3, the program always allows for interceptor homing in calculating attack times. Because this approach is strictly appropriate only when the C^3 provides continuous vectoring information update, there will generally be an error in the attack time estimates, given only periodic or no vectoring information update. Nevertheless, for most cases of interest, the error will be small. Aside from the attack time calculation, the program estimates expected kill probability in a manner consistent with the nature of the C^3. It incorporates a simplistic "cookie-cutter" model for both the interceptor's lethal envelope and the sensor coverage. For example, the conventional kill probability is taken to be zero outside the weapon range and constant inside the weapon range, independent of azimuthal angle. At his discretion, the user can fold in more complicated envelopes.

Penetrators are assumed to fly at constant altitude from the point at which they penetrate the warning network fence until they reach their target location. The amount of maneuvering that the penetrator does is determined by the ratio of the total amount of fuel available for this segment of the flight to the amount needed to fly the segment in a straight line. This ratio should be greater than or equal to one, or the penetrator would run out of fuel before it reached its target. Since the degree of maneuvering determines the effective velocity of the penetrator between the fence penetration point and its target, the program calculates the fence penetration time based on the time the penetrator is to be at the target. The program also has the capability to simulate simultaneous target attacks by all the penetrators.

The program determines its own start time for the scenario. The start time is the earliest penetrator fence crossing time plus a scramble time for the interceptors. No penetrators are attacked after they reach their target.

Although the coordinate system for the model is cartesian, the tracking sensor coverage is simulated in a spherical coordinate system to properly account for horizon masking of low penetrators.

Three types of interceptor bases may be specified in the model: (1) bases with refueling and weapon loading facilities, (2) bases with refueling facilities, and (3) bases with runways only. The model will always insure that the interceptor is able to land at a base upon completing its mission. The model will try to find a base for the interceptor to land in the order given above. If an interceptor lands at a type 1 base, it is refueled, reweaponed, and is again ready to engage penetrators. If an interceptor with no remaining weapons lands at a type 2 base and there is a type 1 base within its operating range, the interceptor is flown to that base, refueled, reweaponed, and is again ready to engage penetrators. Otherwise, it is dropped from the problem. If the interceptor has some weapons left, it is refueled and is again ready to engage penetrators.

If the interceptor is forced to land at a type 3 base, it is dropped from the problem because of lack of fuel. At the start of the problem the interceptors are assumed to be fully loaded with fuel and weapons, and can therefore use any type of base initially. The model only accommodates interceptors initially located at one base in a single problem. Problems with multiple basing are easily accommodated by running multiple problems that build on the results of previous cases. This is done by not zeroing the kill probabilities for the penetrators between problems and is user controllable. The first interceptor is able to takeoff at the problem start time, and successive interceptors at specified intervals thereafter. The model assumes there will be no landing and takeoff conflicts between the interceptors later in the problem. The interceptors will not actually leave the base for their first engagement until the target first enters a tracking sensor coverage so that the interceptor can be vectored to the engagement point. The interceptor is always vectored to the target that can be engaged earliest, but it cannot attack the same target successively. Targets are considered killed when their cumulative

kill probability exceeds a user-determined confidence level. The interceptor can attack from it cruise altitude or can be forced to dive to the penetrator altitude for the attack and return to the cruise altitude between attacks.

B. INPUT. Input to the APVAST program is based on cards containing an identifier and, generally, data associated with the identifier. The identifier may be the name of a variable in the model. The first ten spaces on the card are used for the identifier, left justified, followed by two ten column fields for floating point data. The remainder of the card may be used for comments. In many instances, this format is not adequate to allow the specification of all data associated with the identifier. In these cases, the identifier card is immediately followed by additional specially formatted data cards. The order of the identifier cards within a data deck is not important, although cards associated with an identifier card must be in proper order. A specific case is set up by defining all the necessary information for the model with the identifier cards and their associated cards. The case is terminated by the identifier "ENDCASE." Multiple cases may be run by the model. Once data are defined by an identifier card, they may be changed by specifying new data with another identifier card with the same identifier name. Data which does not change from case to case need only be input once. Additional cases may be defined by changing parameters of the previous data set, thus simplifying the generation of multiple cases. Program execution is immediately terminated by the identifier "ENDJOB." The program prints out all the input data to provide a permanent record of the parameters associated with each run. Data appearing on cards associated with the identifier card are labeled in the output with variable names or descriptions. Parameter names and descriptions are given in this section in addition to the identifier names to help describe the input to the model. The model checks for invalid identifier names and will issue a diagnostic message and terminate execution when one is found.

Organizations desiring copies of the computer code should complete the attached Statement of Terms and Conditions, Release of Air Force-Owned or Developed Computer Software, and send the request to the Directorate of Aerospace Studies, Kirtland AFB, New Mexico 87117.

STATEMENT OF TERMS AND CONDITIONS

RELEASE OF AIR FORCE-OWNED OR DEVELOPED COMPUTER SOFTWARE

DATE_____

1. In accordance with the provisions of AFR 300-6, release of the following U.S. Air Force software package (computer programs, systems descriptions, and/or documentation) is requested:

2. The requested software package will be used for the following purposes:

Such use is projected to accrue benefit to the Government as follows:

3. I/we will be responsible for assuring that the software that we received will not be used for any purpose other than shown in paragraph 2 above; also, it will not be released to anyone without the prior approval of the Air Force. Further, the release of the requested software package will not result in competition with other software packages offered by commercial firms.

4. I/we guarantee that the provided software package, and/or any modified version thereof, will not be published for profit or in any manner offered for sale to the government; it will not be sold or given to any other activity or firm, without the prior written approval of the Air Force. If this software is modified or enhanced using government funds, the Government owns the results, whether the software is the basis of, or incidental to a contract. The Government shall not pay a second time for this software or the enhanced/modified version thereof. The package may be used in contract with the Government but no charge may be made for its use.

5. The U.S. Air Force is neither liable nor responsible for maintenance, updating or correction of any errors in the software package provided.

6. I/we understand that no material subject to national defense security classification or proprietary right was intended to be released to us. I/we will report promptly the discovery of any material with such restrictions to the Air Force approving authority. I/we will follow all instructions concerning the use or return of such material in accordance with regulations applying to classified material, and will make no further study, use or copy such material subject to security or proprietary rights marking.

7. I/we understand that the software package received is intended for domestic use only. It will not be made available to foreign governments nor used in any contract with a foreign government.

Signature of Requestor	Signature of Air Force Approving Authority
Name/Title of Requestor	Name/Title of Air Force Approving Authority
Organization/Address	Organization/Location
City, State and Zip Code	

LIST OF ACRONYMS AND SYMBOLS

A	Point from which Penetrator is Attacked ("Attack Point")
<A>	Expected Attack Point
<A'>	Expected Intermediate Attack Point (see figure 11)
A*	Previous Attack Point
AAM	Air-to-Air Missile
AB	Air Base of Interceptor
AFCMD/SA	Air Force Contract Management Division/Studies and Analyses -- Office Symbol of the Directorate of Aerospace Studies
a	Characteristic Distance of Extreme Maneuver (see figure 5)
C	Cosine of the Total Heading (see equation (30d))
C^3	Command, Control, and Communications
CHDF	Change-of-Heading Distribution Function
CSDF	Change-of-Speed Distribution Function
d	Separation between Interceptor and Penetrator (see figure 8)
erfc(x)	Complementary Error Function
$\vec{e}_x$, $\vec{e}_y$	Basic Vectors of Air Base-Centered Cartesian Coordinate System (see figure 7)
F	Fence, Tactical Warning (See figures 1-3)
G_x, G_y	Kernels of Convolution Integrals (see equations 36))
HDF	Heading Distribution Function
h	Penetrator Cruising Altitude
h_I	Interceptor Cruising Altitude
K	Point at which Penetrator is Killed
<K>	Expected Point of Penetrator Kill
L	Expected Penetrator Path (see figure 3)
M	Orthonormal Transformation Matrix (see equation A7c))
$\vec{m}$	Missile Transit Vector (see figure 12)

$<N_k>$	Expected Number of Penetrators Killed
N_x, N_y	Normalization Constants (see equations (B15))
PDF	Position Distribution Function
$P(t)$	Penetrator Position at Time t
$\hat{P}(t)$	Sensor-Observed Penetrator Position at Time t
$<\hat{P}(t)>$	Expected Sensor-Observed Penetrator Position at Time t
P_F	Point of Fence Penetration
P_H	Location of Penetrator Home Base
$<\hat{P}_I(t)>$	Expected Interceptor Position at Time t
P_K	Conventional Kill Probability
$<P_K>$	Expected Kill Probability
P_T	Location of Penetrator's Target
Q	Penetrator Position at Start of Attack (see figure 7)
$Q(x)$	Gaussian Probability Function
q	Interceptor Weapon Load
R_{BF}	Distance between Penetrator's Home Base and the Fence (see figure 1)
R_{FT}	Distance between Fence and Penetrator's Target (see figure 1)
R_I	Total Interceptor Range
$R_I(t)$	Cumulative Interceptor Range Expended at Time t
R_M	Operational Range of Missile
R_P	Total Penetrator Range
R_{TR}	Distance between Penetrator's Target and Penetrator's Recovery Base (see figure 1)
$\vec{r}_A$	Radius Vector to Point A
$\vec{r}_{A^*}$	Radius Vector to Point A*
	Radius Vector to Point A'
	Radius Vector from Air Base to Penetrator (see figure A2)
	Radius Vector from Air Base to Surveillance Sensor (see

$\vec{r}_C$	Climb Vector (see figure 9)
$\vec{r}_D$	Dive Vector
$\vec{r}_Q$	Radius Vector to Point Q (see figure 7)
$\vec{r}_{SP}$	Radius Vector from Surveillance Sensor to Penetrator (see figure A2)
S	Sensor
S	Sine of Total Heading (see equation (30c))
SDF	Speed Distribution Function
$\vec{T}$	Penetrator Transit Vector (see figure 7)
$\vec{T}_I$	Interceptor Transit Vector (see figure 7)
TSDF	Total Speed Distribution Function
t_A	Attack Time
t_A'	Projected Attack Time
t_F	Time at which Penetrator Crosses Fence
t_{IN}	Intermediate Time (see equation (97))
t_K	Kill Time
t_T	Time of Penetrator Attack against US Target
t_a	Time Interceptor Arrives at Point A
t_ℓ	Time Interceptor Leaves Point A*
$V[v]$	Total Speed Distribution Function
$\hat{V}[\hat{v}]$	Speed Distribution Function
$\overset{+}{V}[\overset{+}{v}]$	Change-of-Speed Distribution Function
$v(t)$	Penetrator Speed at Time t
$\hat{v}(t)$	Sensor-Observed Penetrator Speed at Time t
$\langle\hat{v}\rangle$	Expected Sensor-Observed Penetrator Speed
v	Maneuver-Induced Change in Penetrator Speed
$\langle\overset{+}{v}\rangle$	Expected Maneuver-Induced Change in Penetrator Speed
v_C	Interceptor Climb Speed
v_D	Interceptor Dive Speed

v_e	Penetrator Speed along its Expected Path
V_I	Interceptor Speed
V_{Ie}	Interceptor Speed along its Expected Path
V_M	Missile Speed
(v_r, v_θ, v_ϕ)	Penetrator Velocity Components in Spherical Coordinates (see equation (A7b))
(v_x, v_y, v_z)	Penetrator Velocity Components in Cartesian Coordinates (see equation (A6b))
$\vec{W}$	Auxiliary Vector in Attack Time Solution (see equation (57))
$\vec{W}_M$	Auxiliary Vector in AAM Attack Time Solution (see equation (99b))
W_x, W_y	Cartesian Components of W
$\hat{X}[\hat{x}(t)]$	Position Distribution Function
$X_i, \hat{X}_i, \overset{+}{X}_i$	Terms in Convolution Integral Expansion (see equations (37))
(x, y, z)	Cartesian Coordinate System Centered on the Interceptor Air Base
$(\hat{x}, \hat{y}, \hat{z})$	Sensor-Observed Penetrator Coordinates
$(<\hat{x}>, <\hat{y}>, <\hat{z}>)$	Expected Sensor-Observed Penetrator Coordinates
(x_A, y_A, z_A)	Coordinates of Attack Point A
(x_A^*, y_A^*, z_A^*)	Coordinates of Attack Point A*
(x_{BP}, y_{BP}, z_{BP})	Cartesian Components of $\vec{r}_{BP}$
(x_{BS}, y_{BS}, z_{BS})	Cartesian Components of $\vec{r}_{BS}$
(x_F, y_F, z_F)	Coordinates of Point P_F
(x_Q, y_Q, z_Q)	Coordinates of Point Q
(x_S, y_S, z_S)	Cartesian Coordinate System Centered on the Surveillance Sensor
(x_{SP}, y_{SP}, z_{SP})	Cartesian Components of $\vec{r}_{SP}$
(x_T, y_T, z_T)	Coordinates of point P_T
$\hat{Y}[\hat{y}(t)]$	Position Distribution Function
$Y_i, \hat{Y}_i, \overset{+}{Y}_i$	Terms in Convolution Integral Expansion (see equations (37))

$\hat{Z}[\hat{z}(t_i)]$	Position Distribution Function
α_C, α_D	Auxiliary Terms in Flight Profile Calculations (see equations (75))
β	Angle between $\vec{T}_{I1}$ and $\vec{T}_{I2}$ (see figure 10)
γ_C	Interceptor Climb Angle
γ_D	Interceptor Dive Angle
$\Delta x, \Delta y$	Auxiliary Terms in Convolution Integral Expansion (see equations (37))
Θ	Auxiliary Time in Attack Time Calculations (see equation (58))
(θ, ϕ)	Angular Penetrator Coordinates with respect to the Surveillance Sensor (see figure A1)
$(\hat{\theta}, \hat{\phi})$	Sensor-Observed Angular Penetrator Coordinates
$\hat{\mu}$	Tangent of the Sensor-Observed Penetrator Heading
$\ddagger{\mu}$	Tangent of the Manuever-Induced Penetrator Heading Change
ξ	Characteristic Angle of Extreme Manuever (see figure 5)
$\rho(t)$	*Auxiliary Term in Convolution Integral Expansion* (see equation (32c))
σ_C, σ_S	Auxiliary Terms in Position Distribution Functions (see equations (33))
$(\sigma_R, \sigma_{EL}, \sigma_{AZ})$	Standard Deviations in Measurements of (r_{SP}, θ, ϕ)
$\hat{\sigma}_v$	Standard Deviation in Penetrator Speed Measurement
$\ddagger{\sigma}_v$	Maneuver-Induced Uncertainty in Penetrator Speed
$(\sigma_{vR}, \sigma_{vEL}, \sigma_{vAZ})$	Standard Deviations in Measurements of (V_r, V_θ, V_ϕ)
σ_v	Standard Deviation in Total Penetrator Speed (see equation (26b))
$(\hat{\sigma}_x, \hat{\sigma}_y, \hat{\sigma}_z)$	Standard Deviations in Measurements of (x,y,z)
$\hat{\sigma}_z^*$	Auxiliary Term in Position Distribution Function (see equation (36))
$(\sigma_{xS}, \sigma_{yS}, \sigma_{zS})$	Standard Deviations in Measurements of (x_{SP}, y_{SP}, z_{SP})
$\hat{\sigma}_\psi$	Standard Deviation in Penetrator Heading Measurement

$\overset{+}{\sigma}_{\psi}$	Maneuver-Induced Uncertainty in Penetrator Heading
τ_C	Interceptor Climb Time
τ_D	Interceptor Dive Time
τ_d	Dead Time
τ_{LAG}	Lag Time in Interceptor's Transit from Point A* to Point A Induced by Flight Profile
τ_L	Loiter Time
τ_M	Missile Flight Time
τ_S	Search Time
τ_v	Period between Successive Updates of Vectoring Information
$\hat{\Psi}[\hat{\psi}, t]$	Heading Distribution Function
$\overset{+}{\Psi}[\overset{+}{\psi}]$	Change-of-Heading Distribution Function
ψ	Penetrator Heading
$\hat{\psi}$	Sensor-Observed Penetrator Heading
$\langle\hat{\psi}\rangle$	Expected Sensor-Observed Penetrator Heading
$\overset{+}{\psi}$	Maneuver-Induced Change of Penetrator Heading
$\langle\overset{+}{\psi}\rangle$	Expected Maneuver-Induced Change of Penetrator Heading


DAT
FILM
2